Precambrian Research 375 (2022) 106671

Contents lists available at ScienceDirect

Precambrian Research

journal homepage: www.elsevier.com/locate/precamres

# Understanding the Paleoproterozoic Circum-Superior Large Igneous Province constrains the thermal properties of Earth's mantle through time

Claude Herzberg *

*Department of Earth and Planetary Sciences, Rutgers University, 610 Taylor Road, Piscataway, NJ 08854, USA*

ARTICLE INFO

*Keywords:*
Circum-Superior Large Igneous Province
Basalt
Komatiite
Mantle potential temperature

ABSTRACT

Basalts and komatiites in the ~1880 Ma Paleoproterozoic Circum-Superior Large Igneous Province are associated in space and time with the closure/subduction of the Manikewan ocean and formation of the Trans-Hudson Orogen during the construction of Laurentia and the supercontinent of Nuna/Columbia. In one model, the igneous rocks formed by the melting of ambient mantle during contemporaneous closure of the Manikewan ocean and rifting of the margins of the Superior craton. In another model melting took place in a mantle plume. Resolution to this problem can help in the understanding of the role of LIPS in supercontinent assembly or breakup over the last 2 billion years of Earth history. It can also constrain the thermal properties of ambient mantle and mantle plumes over the last 3.5 billion years. The contrasting hypotheses were tested by petrological modeling of a large database of basalts and komatiites from the Circum-Superior Large Igneous Province. Results reveal limited variability in mantle potential temperature, from 1540 to 1570 °C, over ~12 to 15 million years in time and over 1500 km in space from the Cape Smith Belt in the north to the Winnipegosis Belt in the southwest. The essential problem with the mantle plume model for the Circum-Superior LIP is that it predicts thermal heterogeneity, in contrast with the evidence presented here; there is no Phanerozoic mantle plume analog. The limited long wavelength variation in $T_P$ is characteristic of ambient mantle magmatism, evidence supporting the plate tectonic model for the Circum-Superior LIP. Results are consistent with ambient mantle thermal models characterized by sluggish mantle convection in the past and with a present-day Urey ratio of about 0.38 (Korenaga, J. 2008. Urey ratio and the structure and evolution of Earth's mantle. Rev. Geophys. 46, RG2007). In contrast, most high MgO komatiites in Paleoproterozoic and Archean greenstone belts melted from sources that were ~100–200 °C higher. This temperature excess is similar to 100–250 °C for most Phanerozoic mantle plumes, demonstrating approximate constancy of thermal properties of mantle plume structures through time.

## 1. Introduction

The belt of mafic and ultramafic rocks that is discontinuously distributed over 3400 km around the Superior craton (Fig. 1) is called the Circum-Superior Belt (Baragar and Scoates, 1981). In the Cape Smith Belt to the north (Fig. 1), there is a ~120 Ma time span between the oldest rocks at 1998 Ma (Kastek et al., 2018) and the youngest at 1881.5 Ma (Bleeker and Kamo, 2018). Similarly in the Thompson Nickel Belt to the southwest, ages range from ~2100 Ma (Heaman et al., 2009) to 1880 Ma (Hulbert et al., 2005; Scoates et al., 2017), a ~220 Ma time-span. Elsewhere in the Circum-Superior Belt the ages are more restricted to ~1880 Ma, a synchronicity that led Ernst and Buchan (2004) to conclude that these members of the Circum-Superior Belt are a large igneous province, now often referred to as the Circum-Superior Large Igneous Province, or CSLIP (e.g., Minifie et al., 2013; Ciborowski et al., 2017). Thus, the CSLIP is now considered to be distinct from the Circum-Superior Belt in having an age of ~1880 Ma; however, evidence presented in this work indicates it may have been a late-stage part of a magmatic continuum that started hundreds of millions of years earlier.

Tectonically, the CSLIP is associated in space and time with the closure of the Manikewan ocean and formation of the Trans-Hudson Orogen during the construction of Laurentia (Percival et al., 2005; Corrigan et al., 2009). It is one of a global distribution of LIPS associated with collisional orogens that sutured cratons together during the assembly of the Nuna/Columbia supercontinent (French et al., 2008; Condie et al., 2021). In contrast, Phanerozoic LIPS are associated with continental rifting, breakup, and seafloor spreading (e.g., Coffin and Eldholm, 1994; Storey, 1995; Courtillot et al., 1999; Saunders et al.,

* Corresponding author.
*E-mail address:* herzberg@eps.rutgers.edu.

https://doi.org/10.1016/j.precamres.2022.106671
Received 7 January 2022; Received in revised form 18 March 2022; Accepted 18 March 2022

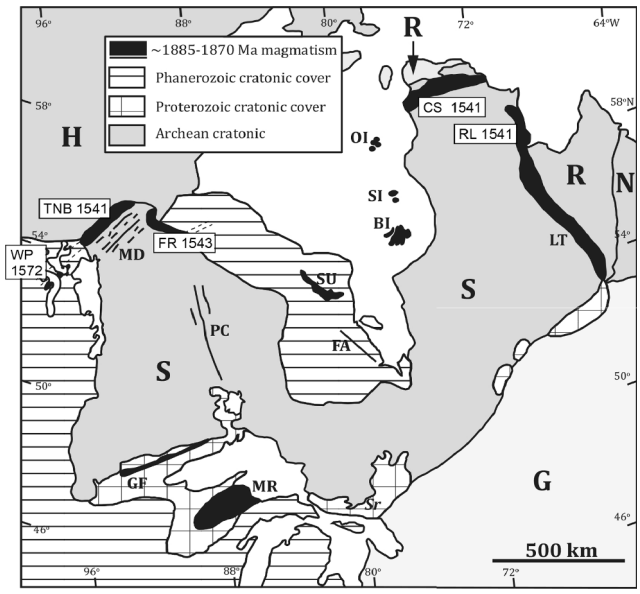


**Fig. 1.** Map showing the locations of members of the Circum-Superior Large Igneous Province, modified from Ciborowski et al. (2017). CS – Cape Smith Belt, RL – Roberts Lake, LT – Labrador Trough, TNB – Thompson Nickel Belt, MD – Molson dykes, WP – Winnipegosis Belt, FR – Fox River Belt, BI – Belcher Islands, FA – Fort Albany dykes, GF – Gunflint Formation, MR – Marquette Range Supergroup, OI – Ottawa Islands, PC – Pickle Crow dyke, SI – Sleeper Islands, SU – Sutton Inlier. Archean cratons: S – Superior, H – Hearne, N – Nain, R – Rae. G – Proterozoic Grenville Province. Numbers with location identifiers are mean mantle potential temperatures $T_P$ summarized in Table 1.

1997; Buiter and Torsvik, 2014; Larsen and Williamson, 2020; Condie et al., 2021). Studies of the Circum-Superior Large Igneous Province can therefore potentially help in the understanding of the role of LIPS in supercontinent assembly and/or breakup over the last 2 billion years of Earth history (Condie et al., 2021).

French et al. (2008) and Heaman et al. (2009) highlighted the association of widespread magmatism with intracontinental rifting and basin development around the Superior craton during closure and subduction of the Manikewan ocean; this is a plate tectonic model for the CSLIP wherein melting occurred during passive upwelling of upper ambient mantle asthenosphere. A plate tectonic model was similarly offered by Corrigan et al. (2009) to explain the penecontemporaneous relationship between the ~1880 Ma rocks of the CSLIP and continental arc type calc-alkaline plutons in the northwestern margin of the Superior craton.

In contrast, the mantle plume model is currently favored (Ernst and Bleeker, 2010; Minifie et al., 2013; Ciborowski et al, 2017; Waterton et al., 2017; Kastek et al., 2020; Bleeker and Kamo, 2020; Barnes et al., 2021; Condie et al., 2021). Advocates of the mantle plume model do not address the association of the CSLIP with the destruction of the Manikewan ocean and construction of Laurentia. And some authors suggest that it was a single mantle plume, not multiple plumes, that formed the CSLIP (Minifie et al., 2013; Ciborowski et al, 2017; Bleeker and Kamo, 2020).

The purpose of this paper is to review the evidence for the origin of the Circum-Superior LIP, whether it formed by melting of ambient mantle in a plate tectonic setting or by melting in a mantle plume. Resolution to this problem has important global implications. An origin by ambient mantle melting would help to constrain the thermal history of the Earth. In the hot ambient mantle model of Korenaga (2008) and Herzberg et al. (2010), the basalts and komatiites of the CSLIP would be samples of igneous rocks characteristic of ancient oceanic crust and continental rifts. In cooler ambient mantle models (Davies, 2009; Ganne and Feng, 2017; Aulbach and Arndt, 2019), such rocks would have been produced in mantle plumes, the presently preferred model for the CSLIP.

Rocks occupying the Circum-Superior Large Igneous Province occur as extrusive basalts and komatiites as well as intrusive dykes and sills (e.g., Heaman et al., 2009; Desharnais et al., 2004; Ciborowski et al, 2017). Unlike the CSLIP, rocks in all other LIPS associated with Nuna/Columbia assembly are found strictly in dykes (see Condie et al., 2021 for compilation). The distinction is important because inferences regarding conditions of melting in the mantle can only be obtained through petrological modeling of solidified basaltic/komatiitic liquids found in lava flows, not cumulate lithologies in dykes and sills (e.g., Herzberg and Asimow, 2015). The basalts and komatiites of the Circum-Superior LIP are uniquely important for constraining the conditions of melting in the mantle during the ~1880 Ma time frame of the Paleoproterozoic.

The approximate synchronicity at 1880 Ma for the CSLIP is considered to be evidence for the mantle plume model. In contrast, a wider spectrum of ages is expected of the plate tectonic model. However, eruption ages of volcanic rocks are typically inferred from U-Pb dates obtained on intrusive rocks found in spatially associated dykes or sills (Heaman et al. 2009), and the assumption, typically implicit, is made that both were part of a contemporaneous magmatic plumbing system. Careful field studies can test this assumption (e.g., Bleeker and Kamo, 2020). But should it fail, the timing of volcanism will be a minimum age, potentially compromising the mantle plume model that requires a short magmatic duration. In this work, it is assumed that the ages of volcanic rocks are similar to reported ages of intrusive igneous rocks.

The challenge is to use the compositions of basalts and komatiites to constrain the temperature of the mantle source, the "mantle potential temperature", $T_P$ (McKenzie and Bickle, 1988). This is the temperature that the adiabatically convecting mantle asthenosphere would be at the surface if it did not melt during decompression. It is a fixed pressure reference frame for quantitatively comparing hot from cold mantle sources that melt to produce magmas. Melts produced in the mantle are called "primary magmas", and their MgO and FeO contents are important to determine because they increase with mantle potential temperature $T_P$ (Langmuir et al., 1992; Putirka et al., 2007; Herzberg and O'Hara, 2002). But they are always modified by fractional crystallization owing to heat loss during transit to the crust. Restoration of the primary magma composition from these differentiated lavas is the primary magma problem in igneous petrology. The problem is tractable for erupted basalts and komatiites that only differ in composition from their primary magmas by olivine crystallization. These primitive volcanic rocks have high MgO contents and are common in the Circum-Superior Large Igneous Province.

The petrological method used in this paper for calculating primary magma composition and mantle potential temperature is based on the PRIMELT3 model of Herzberg and Asimow (2015). This method is described in the following in Section 2 and special attention is devoted to its strengths and weaknesses. PRIMELT3 was implemented on basalt and komatiite whole rock compositions from the Circum-Superior LIP and solutions for primary magma compositions and mantle potential temperatures $T_P$ are given in Section 3. Results are then compared with the thermal properties of ambient mantle in Section 4. A review follows in Section 5 of the thermal properties of Precambrian mantle plumes and how much hotter they were compared with ambient mantle. With this background information in place, together with a review of studies on the thermal and temporal properties of modern mantle plumes, a critical evaluation is made of the mantle plume model for the Circum-Superior LIP in Section 6. Finally, Section 7 discusses a plate tectonic alternative to the mantle plume model.

## 2. Petrological method

### 2.1. PRIMELT3 for basalts and low MgO komatiites of the circum-superior LIP

PRIMELT3 is used to solve the primary magma problem for basalts

and low MgO komatiites having MgO > 9–10% and < 23%, limits imposed by its calibration; see discussion in section 2.1.2. Herzberg et al. (2010) used PRIMELT2 software of Herzberg and Asimow (2008) to infer the thermal state of the mantle that yielded the Chukotat Group basalts, as did Minifie et al. (2013) on the Fox River member of the CSLIP. In a follow up study Ciborowski et al. (2017) used the PRIMELT3 upgrade of Herzberg and Asimow (2015) on basalts from the Chukotat Group, Winnipegosis, Fox River, Molson dykes, and Emperor volcanics. In this study, PRIMELT3 will continue to be applied on the CSLIP members investigated by Ciborowski et al. (2017); it will also be used on samples from the Thompson Nickel Belt (Zwanzig, 2005) and the Roberts Lake Syncline, located between the Cape Smith fold belt and the Labrador Trough (Kastek et al., 2020). PRIMELT3 was run on 425 whole rock basalt and komatiite compositions. Of these there were 86 successful primary magma solutions and results are summarized according to locality in Table 1. Most lavas yielded unsuccessful primary magma solutions that had compositions outside the calibration of the software, as discussed below. Original whole rock compositions and PRIMELT3 solutions are listed separately in Appendix A.

### 2.1.1. PRIMELT3 strengths

The following information is provided by PRIMELT3: 1) primary magma composition, 2) mantle potential temperature $T_P$, 3) olivine liquidus temperature $T_{OL}$ at 1 atmosphere, 4) melt fraction, 5) residual lithology, 6) Fe-Mg partition coefficient ($K_D$) between olivine and primary magma (i.e., $(FeO/MgO)_{Ol}/(FeO/MgO)_{melt}$) at 1 atmosphere, and 7) Mg# (i.e., molar 100MgO/(MgO + FeO) of olivine in equilibrium with the primary magma composition at 1 atmosphere.

PRIMELT3 provides solutions for batch melting, wherein a partial melt in the mantle is in equilibrium with its residue at all melt fractions. However, it is overly simple because partial melts drain from their sources by buoyant porous flow and matrix compaction at low melt fractions during decompression (Ahern and Turcotte, 1979; McKenzie, 1984). Mixing of such melts produces an accumulated fractional melt. PRIMELT3 solutions for accumulated fractional melting (Herzberg and Asimow, 2015) are used here because they are more physically realistic. For primary magmas from the CSLIP, batch melts are typically higher in MgO than accumulated fraction melts by about 2%, yielding $T_P$ that is too high by about 50 °C.

For primary magmas produced by accumulated fractional melting, olivine liquidus temperature at 1 atmosphere ($T_1^{Ol/L}$) and mantle potential temperature ($T_P$) have been calibrated from their weight % contents of MgO (Herzberg and Asimow, 2015) with the equations:

$$T_1^{Ol/L} = 1020 + 24.4\ MgO - 0.161\ MgO^2 \quad (1)$$

$$T_P = 1025 + 28.6\ MgO - 0.084\ MgO^2 \quad (2)$$

Mantle potential temperature can be related to olivine liquidus temperature (Herzberg and Asimow, 2015) with the equation:

$$T_P = 1.049\ T_1^{Ol/L} - 0.00019\ (T_1^{Ol/L})^2 + 1.487 \cdot 10^{-7}(T_1^{Ol/L})^3 \quad (3)$$

Eq. (1) can reproduce MELTS temperatures (Ghiorso and Sack, 1995) to within ±7 °C. It is usually within 10 °C of the Beattie (1993) thermometer encoded in PRIMELT3 worksheets for primary magma solutions. Eq. (2) has an uncertainty in $T_P$ of ±42 °C (Herzberg and Asimow, 2015). As discussion in Section 5.5, Eq. (3) is useful for estimating how the effect of $H_2O$ on lowering olivine liquidus temperature is propagated to mantle potential temperature (e.g., Sobolev et al., 2016).

The PRIMELT algorithm differs from the commonly used method of calculating primary magma composition by incremental addition of olivine until it is in equilibrium with a target olivine with the highest observed Mg# (e.g., Arndt, 1986; Nisbet et al., 1993). As discussed in section 2.2, this is the method of choice for Precambrian komatiites having compositions outside the PRIMELT calibration bounds. The two methods may agree when primary magma olivine crystals were preserved in a lava flow; an example is given below for Winnipegosis komatiites from the Circum-Superior LIP. However, a disadvantage of this method is that it will underestimate primary magma MgO content if applied to olivines that crystallized from differentiated rather than primary magmas. And this method will fail in cases where olivine is not preserved during metamorphism; in this situation, the Mg# of olivine is often assumed. As an example, mantle potential temperatures $T_P$ can vary by about 100 °C depending on whether the target olivine Mg# is assumed to be 90.0 or 92.0.

### 2.1.2. PRIMELT3 limitations

PRIMELT3 has a number of important limitations. Before they are discussed, it is useful to understand how it calculates a primary magma composition. The PRIMELT family of algorithms was calibrated from experiments on nominally volatile-free fertile peridotite KR4003 (Walter, 1998) and its parameterizations (Herzberg and O'Hara, 2002; Herzberg et al., 2007; Herzberg and Asimow, 2008; 2015). For a detailed explanation the reader is urged to consult Fig. 1 in Herzberg and Asimow (2015) and discussion therein. In brief, all possible compositions for melting fertile peridotite KR4003 with residual spinel and garnet peridotite and harzburgite have been parameterized in a forward model, and they are represented as melt fractions in both Ol-An-Qz and FeO-MgO projection space. The inverse model consists of adding or subtracting olivine in 1% increments to or from a basalt/komatiite composition, creating an array of potential primary magma compositions. For each increment, melt fractions are computed in both Ol-An-Qz-Di and FeO-MgO projection spaces. There is only one point on the array where there is a common melt fraction, and this uniquely identifies the primary magma composition; these melt fractions are given in PRIMELT3 worksheets (Appendix A). However, the solution must also satisfy other oxide components of fertile peridotite melting that are not represented in these two projection spaces. Of these, the CaO contents of primary magmas of fertile peridotite are particularly useful because they have a restricted range of compositions (Herzberg and Asimow, 2008; Jennings and Holland, 2015; Tomlinson and Holland, 2021). PRIMELT3 solutions that satisfy these CaO contents, in addition to melt fractions in Ol-An-Qz and FeO-MgO projection spaces, are referred to in this paper as "successful solutions". But there are a number of ways that primary magma solutions can be compromised.

A major limitation is that PRIMELT3 only works on primitive basalts that differed from their primary magmas by olivine-only addition and subtraction. That is, it should be restricted to basalts that are members of an olivine liquid of descent (i.e., Ol LLD), or olivine-control. This restriction excludes most basalts having less than 9–10% MgO owing to plagioclase and augite stability and fractionation. In all cases, these low

**Table 1**
Mean & 2 σ values of PRIMELT3 Primary Magma Solutions for Basalts & Komatiites from the Circum-Superior LIP.

| Location | N solutions | MgO (wt%) | T Ol/L (°C) Beattie (1993) | T Ol/L (°C) eq (1) | Tp (°C) eq (2) | $K_D$ | Ol Mg# | Melt Fraction |
|---|---|---|---|---|---|---|---|---|
| Povungnituk | 1 | 17.5 | 1392 | 1398 | 1500 | 0.30 | 91.6 | 0.26 |
| Chukotat | 19 | 19.1 (2.6) | 1422 (42) | 1428 (46) | 1541 (64) | 0.31 (0.02) | 91.8 (0.4) | 0.32 (0.04) |
| Roberts Lake | 2 | 19.1 (1.2) | 1418 (20) | 1427 (24) | 1541 (32) | 0.31 (0.0) | 91.8 (0.2) | 0.32 (0.0) |
| Winnipegosis | 44 | 20.3 (1.8) | 1442 (34) | 1449 (32) | 1572 (46) | 0.30 (0.0) | 92.0 (0.4) | 0.33 (0.06) |
| Thompson Nickel Belt | 10 | 19.1 (3.4) | 1418 (60) | 1427 (60) | 1541 (84) | 0.31 (0.02) | 91.8 (0.6) | 0.32 (0.10) |
| Fox River | 10 | 19.2 (4.0) | 1414 (72) | 1428 (74) | 1543 (104) | 0.31 (0.02) | 91.8 (1.0) | 0.33 (0.05) |

MgO basalts were filtered and excluded before implementation of PRIMELT3 to the remaining high MgO samples. The effect of augite fractionation is to yield derivative liquids that are high in FeO and low in CaO. If olivine is subsequently added to these derivative liquids, the result will be a high MgO cumulate that is also high in FeO and low in CaO. For these, PRIMELT3 will provide a solution anyway, but it will be "unsuccessful" and flagged with the error code "augite fractionation".

For many Phanerozoic high Mg basalts, such as those from the shield-building volcanoes of Hawaii, whole rock CaO contents can be low, yielding primary magma solutions that are too low in CaO to be partial melts of peridotite KR-4003 and KLB-1 (Davis et al., 2011; Herzberg, 2006, 2011; Herzberg and Asimow, 2008; Jennings and Holland, 2015; Tomlinson and Holland, 2021). These low CaO melts are similar to those expected of some pyroxenite sources (Herzberg, 2006; 2011). PRIMELT3 will calculate a primary composition anyway, but they are flagged as "pyroxenite source … no solution". As discussed below, this is an unlikely interpretation for unsuccessful primary magma solutions from the CSLIP; metamorphic alteration is another way to lower whole rock CaO content.

Whole rock CaO contents may be high owing to augite addition, and application of PRIMELT3 can yield solutions that have CaO contents that are higher than those of primary melts of fertile peridotite; these are also flagged and termed "unsuccessful solutions".

Another limitation is that successful PRIMELT3 solutions are only valid for primary magmas of a volatile-free fertile peridotite source; however, solutions for volatile peridotite are sometimes encountered, and when this happens, they are flagged with a "volatile peridotite" warning.

The oxidation state of iron must also be known, and a value of $FeO/FeO_T$ needs to be specified for the input lava composition. It is assumed that $FeO/FeO_T = 0.90$. This is slightly lower than 0.91 captured by the Kress and Carmichael (1991) algorithm embedded in Rhyolite-MELTS at QFM-1 and 200 bars (Gualda et al., 2012). This $fO_2$ also compares with QFM-1.2 reported for Archean age Belingwe and Alexo komatiites (Sobolev et al., 2016; Asafov et al., 2018). Modern MORB also have $FeO/FeO_T = 0.90$ (Bézos et al., 2021; Gaborieau et al., 2020; Berry et al., 2018). At the more oxidizing condition of QFM, $FeO/FeO_T = 0.86$. For a Chukotat basalt PRIMELT3 solution, a decrease of $FeO/FeO_T$ from 0.90 to 0.86 would propagate to a decrease in the MgO content of the primary magma from 18.86 to 17.80% MgO; use of Eq. (2) shows that inferred mantle potential temperature $T_P$ would drop from 1535 to 1507 °C, well within the uncertainty of PRIMELT3. Nicklas et al. (2019) suggest QFM + 1.2 for Winnipegosis komatiites from the CSLIP, as oxidizing as some modern mantle plumes that have been attributed to the recycling of oxidized subducted lithosphere (Moussallam et al. 2019) However, there is little evidence for recycled crust in the geochemistry of the CSLIP (e.g., Waterton et al., 2017; Barnes et al. 2021). And evidence is presented below that the Winnipegosis komatiites crystallized from a melt having $FeO/FeO_T = 0.90$, equivalent to QFM-0.6.

It is best to reconstruct primary magma compositions by addition of olivine into a lava composition having a lower MgO content. But PRIMELT3 also performs the reconstruction by olivine subtraction from an olivine cumulate. The latter is generally successful when the FeO content of the olivine is similar to that of the melts from which olivine has been extracted; for most CSLIP cases, this applies to olivines having Mg numbers of about 87 to 92. However, it will be shown below for the Fox River case that PRIMELT3 fails when applied to olivine cumulates with low Mg#s.

Finally, all mafic and ultramafic rocks from the Circum-Superior LIP have had their compositions variably altered during metamorphism ranging from the prehnite-pumpellyite, greenschist, amphibolite to granulite facies. Assessing the effects of element mobility during metamorphism is necessary to evaluate the extent to which igneous interpretations can be compromised. It will be shown that this can contribute to uncertainties in the thermal properties of the mantle from which the igneous rocks were formed as partial melts.

### 2.2. PRIMELT3 "Olivine Calculator" for high MgO komatiites

In general, PRIMELT3 cannot solve the primary magma problem on most Precambrian komatiites having MgO > 23% and $Al_2O_3$ < 5% using melt fraction in the algorithm. These are compositional bounds on its calibration from experimental data and its parameterizations, and PRIMELT3 does not extrapolate well. Attempts to use it will typically result in error codes that inform the user that no solutions are possible.

A method for constraining the primary magma composition of high MgO komatiites makes use of olivine Mg# as first introduced in the seminal papers by Arndt (1986) and Nisbet et al. (1993). A calculation is made of the magma composition in equilibrium with olivine having the highest Mg#. PRIMELT3 similarly offers the user the option of calculating primary magma composition with its "Olivine Calculator". In each spreadsheet, olivine is added to and subtracted from an input komatiite composition in 1 wt% increments, and for each derivative composition is given the Mg# of the equilibrium olivine composition in column AH. The calculated olivine composition is simply matched with an observed olivine composition of interest to give the MgO content of the primary magma. Of the parameters that most affect the outcome of these calculations, the most important are the oxidation state of iron (i.e., $FeO/FeO_T$) of the melts and the value of $K_D$ (i.e., $(FeO/MgO)_{Ol}/(FeO/MgO)_{melt}$) used to calculate equilibrium olivine-melt compositions. Examples are given below. PRIMELT3 uses the thermodynamic model of Toplis (2005) for $K_D$, and it is typically close to 0.30 for high MgO komatiitic primary magmas that crystallize olivine at low pressures. The Olivine Calculator was applied to high MgO komatiites from Precambrian greenstone belts, and results are discussed below in Section 5.

## 3. Primary magmas and mantle potential temperatures for the circum-superior LIP

### 3.1. Cape Smith Belt

The Cape Smith Belt (Fig. 1) contains basalts of two broadly different ages and geochemical properties. The oldest are basalts of the Povungnituk Group dominated by the Beauparlant Formation with an age of 1998 ± 6 Ma (Kastek et al., 2018); these are light REE enriched (Francis et al., 1983), with EMORB-OIB characteristics (Kastek et al., 2018). The younger basalts of the Chukotat Group have ages of 1882.7 ± 1.3 Ma (Randall, 2005) and 1883–1882 Ma (Bleeker and Kamo, 2018; 2020) and relatively flat REE but slightly LREE-depleted patterns.

#### 3.1.1. Chukotat Group

A comprehensive database of basalts from the Chukotat Group (Hynes and Francis, 1982; Francis et al., 1983; Picard, 1989; Ciborowski et al., 2017) is shown in Fig. 2a, normalized volatile-free and with $FeO = 0.9FeO_T$. Most samples contain 9–20% MgO, with a restricted range of FeO contents that are characteristic of olivine fractionation from a primary magma. This is an olivine control, or olivine liquid line of descent (i.e., Ol LLD), and it was modeled using the Olivine Calculator in PRIMELT3 for the primary magma composition obtained from sample CHK-MGO14 of Hynes and Francis (1982). A small population of basalts with MgO < 9% display an iron enrichment trend characteristic of clinopyroxene and plagioclase fractionation of tholeiitic basalts, and it is well-modelled with a Rhyolite-MELTS LLD at QFM-1 and 200 bars (Gualda et al., 2012).

Of the 76 samples having MgO > 9%, primary magma solutions were obtained on 19 (Appendix A) and results are summarized in Table 1. The mean primary magma MgO content is 19.1 ± 2.6% (2σ) yielding $T_P$ = 1541 ± 64 °C (2σ); this is similar to 18.9% MgO for the primary magma composition and its LLD shown in Fig. 2a. Primary magma MgO contents are coupled to FeO. Most Chukotat basalts have FeO contents that are within ± 0.5% of the Ol LLD, but there are outliers that have higher FeO contents. In contrast, most Chukotat basalts have CaO contents that are highly scattered and much lower than those defined by the OL LLD

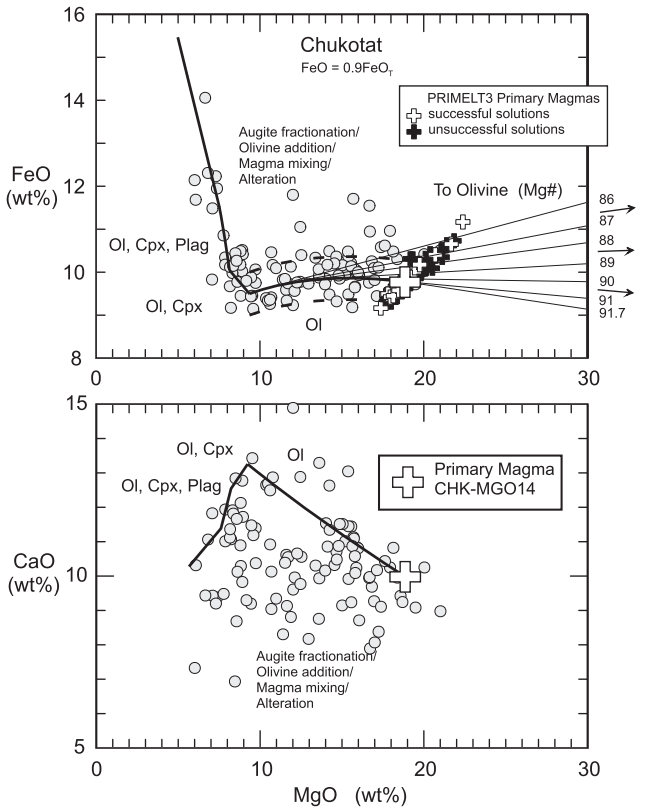


**Fig. 2.** MgO, FeO and CaO contents of Chukotat basalts (filled circles), primary magma solutions (crosses), and model liquid compositions along the liquid line of descent (LLD) for the primary magma composition obtained from CHK-MGO14 of Hynes and Francis (1982; large white filled cross). Primary magmas calculated for basalts with MgO > 9.0%. Numbered straight lines connect liquid compositions on the olivine part of the LLD with their crystallizing olivine compositions indicated by their equilibrium Mg numbers.

(Fig. 2b). For these, application of PRIMELT3 yields solutions that are too low in CaO to be primary accumulated fractional melts of fertile mantle peridotite and are flagged with pyroxenite-source melting; however, this interpretation is not likely because it predicts residual garnet and HREE depletions in the primary melts, which are not observed (Francis et al., 1983; Ciborowski et al., 2017). Augite fractionation and magma mixing can also be discounted because they predict more widespread FeO-enrichment than is observed in Fig. 2a.

It has long been known that Ca is a mobile element during greenschist facies metamorphic alteration of komatiites (e.g., Herzberg, 1992; Nisbet et al., 1993; Lahaye and Arndt, 1996; Robin-Popieul et al., 2012). This is a plausible explanation for the low CaO contents of many of the Chukotat basalts. For these, there is no correlation between CaO and FeO. But that is not to say that metamorphic alteration did not also affect whole rock FeO contents; Robin-Popieul et al. (2012) presented evidence for FeO mobility in komatiites, and its effects could have been random and uncorrelatable with respect to CaO. Some insight into this problem can be gained by work on Alexo and Pyke Hill komatiites of Archean age because, like the Chukotat basalts, the Archean komatiites were metamorphosed in the greenschist facies. Fig. 3 shows data obtained on both whole rock samples (Arndt, 1986; Lahaye and Arndt, 1996; Shore, 1996; Fan and Kerrich, 1997; Sproule et al., 2002; Puchtel et al., 2004; 2009) and olivine-hosted melt inclusions (Sobolev et al., 2016). The variability in $FeO_T$ is approximately ± 0.5% for whole rocks at any given MgO content; in contrast, the variability is more with the limited in the melt inclusion data. The slight offset of melt inclusions to higher $FeO_T$ contents is not relevant to this discussion, but it is likely an artifact of how the melt inclusion data were reconstructed (Sobolev

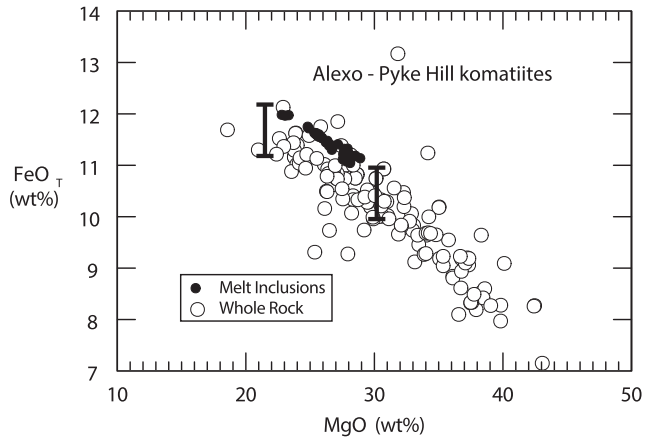


**Fig. 3.** MgO and total FeO contents of Archean komatiites from Alexo and Pyke Hill, Abitibi greenstone belt. Relative to olivine-hosted melt inclusions (Sobolev et al. 2016), whole rocks display a range of FeO contents that reflect iron mobility during greenschist facies metamorphism.

et al., 2016). The important message is that whole rock variability in FeO in Chukotat (Fig. 2a), and all CSLIP samples, is in part a metamorphic rather than a magmatic feature. As primary magma MgO and FeO contents are coupled (Fig. 2a), a ± 0.5% range of FeO contents relative to the Ol LLD for Chukotat basalts propagates to a range in $T_P$ of ± 40 °C, an erroneous variability if it is due to metamorphic alteration.

### 3.1.2. *Povungnituk group*

There is a substantial database of the older basalts from the Povungnituk Group (Hynes and Francis, 1982; Francis et al., 1983; Picard, 1989; Kastek et al., 2018). Except for 6 basalts reported by Kastek et al. (2018), they do not display a clear Ol LLD and are too differentiated to provide PRIMELT3 solutions. The 6 olivine phyric basalts of Kastek et al. (2018) yield pyroxenite or augite fractionation errors, but one basalt from Picard (1989) yielded a successful solution, $T_P$ = 1500 °C (Table 1), similar to those for the much younger Chukotat basalts. As discussed in Sections 3.8 and 8, the similarity in $T_P$ for volcanic rocks with ages that range from 1998 (Kastek et al., 2018) to 1881.5 Ma (Bleeker and Kamo, 2018) is supporting evidence for thermal homogeneity over a 116-million-year lifetime of the Cape Smith Belt. However, additional work is needed on more than one older sample before this conclusion is secure.

## 3.2. *Roberts Lake Syncline*

Lavas from the Roberts Lake Syncline, located between the Cape Smith fold belt and the Labrador Trough (Fig. 1), are mostly low MgO basalts exhibiting a Cpx and Plag LLD defined by FeO enrichment and CaO depletion (Kastek et al., 2020); these are similar to the more differentiated Chukotat basalts for which no successful PRIMELT3 solutions are obtained. However, there are 7 high MgO samples with relatively flat REE but slightly LREE-depleted patterns, also similar to those for Chukotat basalts (Francis et al., 1983). Of these PRIMELT3 yielded 2 successful primary magma solutions, yielding a mean MgO = 19.1% and a mean $T_P$ = 1541 °C (Appendix; Table 1), identical to 19.1% MgO and 1541 °C for the Chukotat basalts. However, working with this low number of successful solutions does not permit a full examination of the ways that they can be compromised. And the ages are not known. However, based on trace and major element geochemical similarities, Kastek et al. (2020) suggested that the Roberts Lake Syncline is a continuation of the Cape Smith belt, a conclusion that is supported by the similarities in their mantle potential temperatures.

### 3.3. Thompson Nickel Belt

About 1500 km to the southwest of the Cape Smith belt are several other members of the Circum-Superior LIP, one of which is the Thompson Nickel Belt (Fig. 1). Reported ages in Ma are: 1880 ± 5 (Hulbert et al., 2005), 1885 ± 49 (Hulbert et al., 2005), 1876.7 ± 5.1 (Heaman et al., 2009) and most recently 1880.2 ± 1.4 by Scoates et al (2017). Lavas from the Bah lake assemblage in the TNB are folded and intensely metamorphosed (Zwanzig, 2005) in the amphibolite to granulite facies (Coueslan et al., 2013). There is a High-Mg suite with relatively flat REE but slightly LREE-depleted patterns (Zwanzig, 2005), similar to the Chukotat basalts (Francis et al., 1983), but they display a greater variability in FeO. Of the 47 samples in this database, there are 10 successful PRIMELT3 primary magma solutions, yielding a mean $T_P$ = 1541 °C, identical to Chukotat. However, there is greater variation in FeO, which propagates to a 2σ variation in $T_P$ of 84 °C, higher than 64 °C for Chukotat (Table 1). As the grade of metamorphism is higher, the greater variability in $T_P$ for the Thomson Nickel Belt is interpreted to reflect Fe mobility, a problem revisited below.

### 3.4. The Winnipegosis Komatiite Belt

The Winnipegosis Komatiite Belt is located in Manitoba, Canada, adjacent to the Thompson Nickel Belt (Fig. 1) and lies beneath 120–500 m of Palaeozoic cover centered beneath Lake Winnipegosis (Waterton et al. 2017). I work with data from drill core samples reported by Waterton et al. (2017). Of the 256 samples provided, some are mineralized, and PRIMELT3 was run on 244 samples that appear least altered. Waterton et al. (2017) reported an age of 1870.3 ± 7.1 Ma, slightly younger than other members of the Circum-Superior LIP. Unlike the Thompson Nickel Belt, Winnipegosis komatiites had undergone a lower degree of metamorphism and deformation, yielding relatively fresh samples with igneous olivine (Waterton et al. 2017). Ciborowski et al. (2017) also provided whole rock data on 17 samples, and these were included in this work.

Whole rock analyses and successful PRIMELT3 primary magma solutions are shown in Fig. 4a. The variability in FeO whole rock compositions is more restricted than for Chukotat basalts, reflecting the relative freshness of these samples, and providing further evidence that metamorphic alteration can indeed compromise magmatic FeO contents. Successful PRIMELT3 solutions were obtained on 44 samples, yielding a mean MgO = 20.3 ± 1.8% (2σ) and $T_P$ = 1572 ± 46 °C (2σ) (Table 1). Sample RP1A-85 from Waterton et al. (2017) provides a solution that is representative of this mean, and its Ol LLD is shown in Fig. 4a. Primary magma MgO contents range from 18.5 to 23.0%, and PRIMELT3 predicts they will crystallize olivines at the surface with Mg numbers of 91.7 to 92.6 (Fig. 5a), the mean being 92.0. PRIMELT3 calculates olivine Mg#s with $K_D$ from the thermodynamic model of Toplis (2005), and it is 0.304 for the mean primary magma composition. For olivine, there is good agreement amongst the PRIMELT3 predicted mean Mg# of 92.0 and the measured maximum Mg# of 92.3 in Winnipegosis olivines (Waterton et al., 2017). However, PRIMELT3 predicts several outliers with Mg#s up to 92.6 (Fig. 5a), an outcome that is discussed below.

Waterton et al. (2017) estimated an MgO content of 23.6% for the primary magma composition, significantly higher than our mean of 20.3%. The calculation was made by determining the composition of the melt in equilibrium with olivine having the highest Mg#, this being 92.3. Their higher MgO result stems from their use of $K_D$ = 0.345, higher than $K_D$ = 0.304 in PRIMELT3. The authors used 0.345 because it is the same as experimental measurements of Matzen et al. (2011) at 1 atmosphere, and the parameterization of Herzberg and O'Hara (2002) of high-pressure experimental data for their primary magma having 23.6% MgO. However, it is notable that subsequent experiments of Matzen et al. (2013; 2017) at 1 atmosphere are typically much lower as shown in Fig. 6. In contrast, $K_D$ is higher in their experiments at elevated

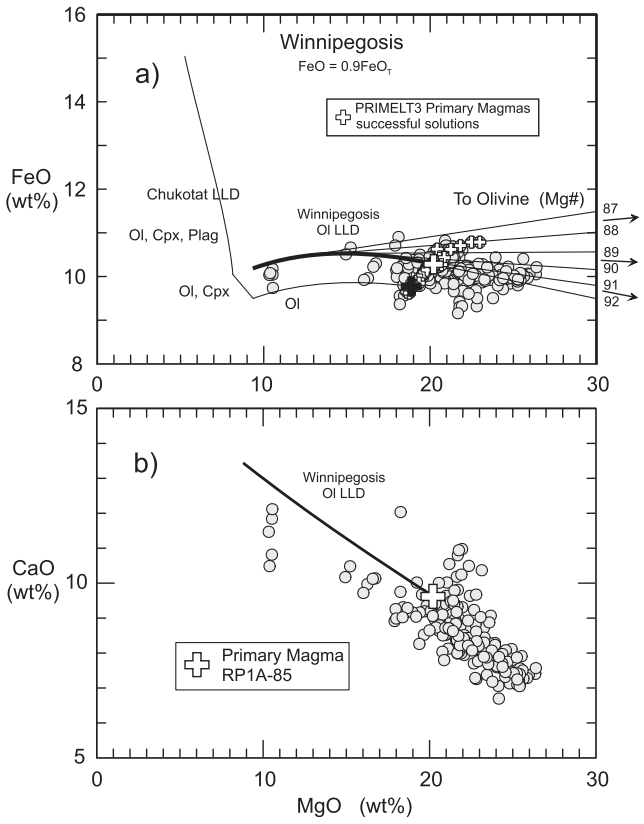


**Fig. 4.** MgO, FeO and CaO contents of Winnipegosis komatiites (filled circles), primary magma solutions (crosses), and model liquid compositions along the olivine liquid line of descent for the primary magma composition obtained from sample RP1A-85 from Waterton et al. (2017; large white filled cross). Numbered straight lines connect liquid compositions on the olivine LLD with their crystallizing olivine compositions indicated by their equilibrium Mg numbers. Large black cross and line emanating from it is the Chukotat primary magma composition shown in Fig. 2 and its LLD, given for comparison.

pressures, 1 to 3 GPa, consistent with the thermodynamic model of Toplis (2005) and the empirical parameterization of Herzberg and O'Hara (2002). The implication is that $K_D$ is ~0.33 to 0.35 at primary magma generation in the mantle, the basis of the PRIMELT forward model (Herzberg and O'Hara, 2002; Herzberg and Asimow, 2008; 2015). However, those primary magmas will crystallize olivine at the surface with a $K_D$ closer to ~0.30, the original Roeder and Emslie (1970) experimental determination at 1 atmosphere. Therefore, we need to know where the Winnipegosis olivines crystallized. It is common to assume phenocryst crystallization at near surface conditions. However, this can now be examined quantitatively from the partitioning of $Al_2O_3$ between olivine and liquid, which is temperature and pressure dependent (Agee and Walker, 1990): $\ln D^{Ol\text{-}L}_{Al2O3} = 0.082P(GPa) - 8290/T(K)$. For Winnipegosis, we calculate $D^{Ol\text{-}L}_{Al2O3}$ = 0.007–0.008 from 0.067% $Al_2O_3$, the mean $Al_2O_3$ in olivine reported by Waterton et al. (2017) and 8.1–9.1% $Al_2O_3$ in Winnipegosis lavas. Primary magmas with 20.3–23.6% have olivine liquidus temperatures of 1449–1495 °C at 1 atmosphere, yielding $D^{Ol\text{-}L}_{Al2O3}$ = 0.008 according to Agee and Walker (1990), identical to that for Winnipegosis and confirming that their olivines crystallized at near-surface conditions. Therefore, the correct $K_D$ to use is ~0.30, not 0.345, and the Winnipegosis primary magma had about 20.3% MgO, not 23.6% MgO. The significance of this attention to detail is its impact on inferred mantle potential temperature: for MgO = 20.3% $T_P$ = 1572 °C; for MgO = 23.6% $T_P$ = 1653 °C, 81 °C higher.

Nicklas et al. (2019) obtained 21.1 ± 2.5% MgO, similar to 20.3 ± 1.8% in this study. In contrast, Ciborowski et al. (2017) used PRIMELT3 to obtain primary magmas with 23.9–24.9% MgO, consistent with the

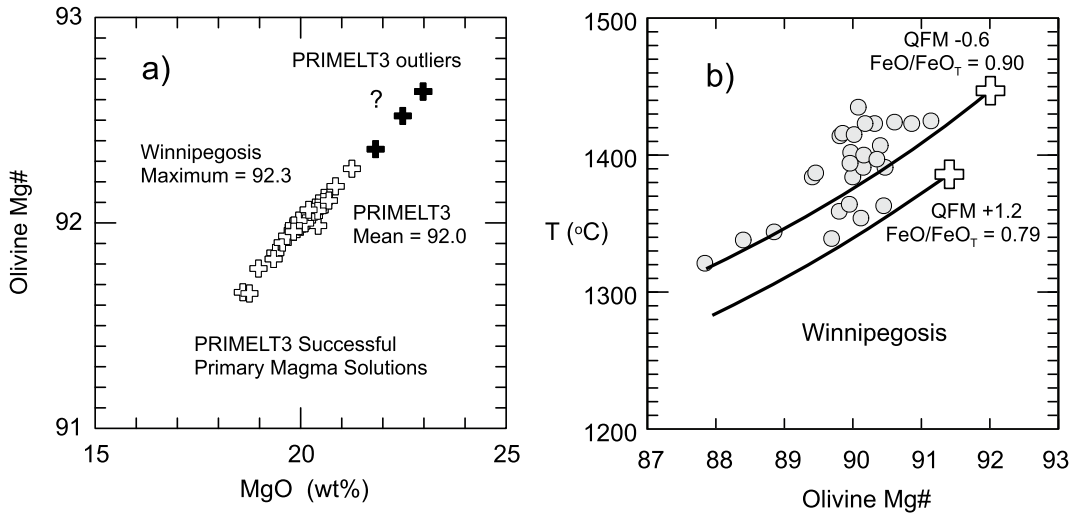


**Fig. 5.** Model and observed olivine Mg numbers and olivine crystallization temperatures for Winnipegosis komatiites. a) PRIMELT3 predicted olivines that would crystallize from primary magmas with the MgO contents shown. b) filled circles are temperatures and mean olivine Mg#s reported by Waterton et al. (2017); large white crosses are PRIMELT3 computed olivine compositions and olivine liquidus temperatures at 1 atmosphere for two assumed oxidation states of iron in the primary magma. Fractional crystallization of olivine from the two primary magmas yields predicted olivine crystallization temperatures and compositions along the two curved lines.

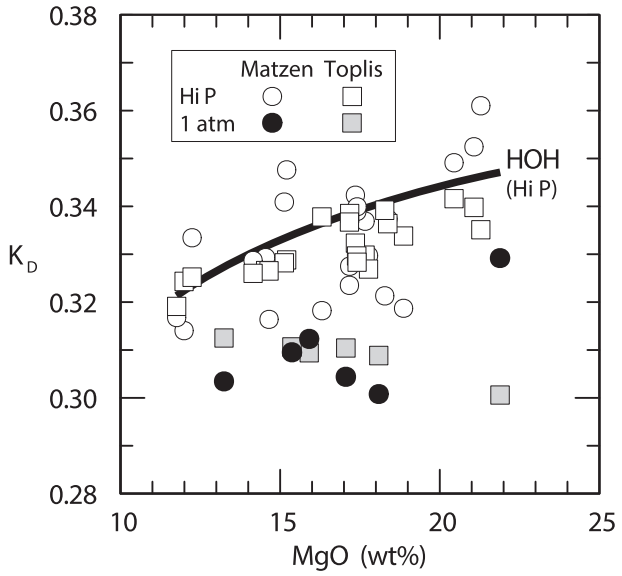


**Fig. 6.** $K_D$ between olivine and liquid (i.e., $(FeO/MgO)_{Ol}/(FeO/MgO)_{melt}$) in melting experiments of Matzen et al. (2013; 2017) compared with their predicted values using the thermodynamic model of Toplis (2005) and the high pressure parameterization of Herzberg and O'Hara (2002). $K_D$ is lower for near-surface olivine crystallization and higher at conditions of melt generation in the mantle.

high MgO contents inferred by Waterton et al. (2017). However, we obtain 19.4–21.9% MgO using PRIMELT3 on their same samples. How is it possible to get different outcomes from the same software applied to the same samples? As discussed in Section 2.1.1, PRIMELT3 offers solutions for primary magmas produced by both accumulated fractional melting and batch melting, and it appears that Ciborowski et al. (2017) used the later which always yields higher MgO contents. However, as also discussed above, this work is restricted to primary magmas produced by accumulated fractional melting because it more accurately reflects the physics of melting of the mantle. Primary magma MgO contents estimated by Ciborowski et al. (2017) for Winnipegosis are too high.

As an independent check on temperature reliability, a comparison is made of temperatures reported by Waterton et al. (2017) obtained by the Al-in-olivine method for olivine-spinel pairs (Coogan et al., 2014) with those obtained from olivine crystallization temperatures using Eq. (1). The primary magma derived from sample RP1A-85 has MgO = 20.21% and FeO/FeO$_T$ = 0.90, the condition at $fO_2$ = QFM −0.6 (Kress and Carmichael, 1991); it will crystallize olivine with Mg# 92.0 at 1447 °C. Subsequent crystallization of olivine along the Ol LLD will yield derivative liquids with lower MgO contents, and these will crystallize olivines with Mg#s at the temperatures shown by the array in Fig. 5b. These temperatures are similar to those determined by Waterton et al. (2017) using the Al-in-olivine method; the offset to slightly lower temperatures than those of spinel saturation arises from slow diffusivity of Al in olivine. The similarities in olivine liquidus and olivine/spinel temperatures have been noted elsewhere (Coogan et al., 2014; Spice et al., 2016). In other cases, such as the Abitibi komattites, olivine/spinel temperatures are lower than olivine liquidus temperatures (Trela et al., 2017). It is notable that the temperature agreement breaks down for more oxidizing conditions. If $fO_2$ = QFM + 1.2 (Nicklas et al., 2019), then FeO/FeO$_T$ = 0.79 (Kress and Carmichael, 1991), the primary magma for sample RP1A-85 has lower FeO and MgO and will crystallize olivine with an Mg# = 91.5 at 1390 °C (Fig. 5b). Fractional crystallization of olivine will yield temperatures that are lower than those obtained by Waterton et al. (2017) (Fig. 5b). This is an independent test of the assumption that the more reduced condition of FeO/FeO$_T$ = 0.90 is a good description of the oxidation state of iron for the Winnipegosis komatiites, in agreement with that independently determined by Waterton et al. (2017).

Winnipegosis lavas display less variation in CaO (Fig. 4b) than do those for Chukotat lavas (Fig. 2b), as expected from their relatively fresh characteristics (Waterton et al., 2017). However, the variations have compromised many PRIMELT3 primary magma solutions, yielding unsuccessful solutions identified with pyroxenite melting, augite fraction and augite accumulation. However, as discussed with Chukotat, most of these unsuccessful solutions are likely the result of metamorphic alteration. And the successful solutions having the highest MgO contents should be considered suspect because PRIMELT3 predicts they would crystallize olivines with MgO # > 92.3, which is not observed (Waterton et al., 2017). Most solutions yielding MgO contents and olivine Mg#s greater than the means of 20.3% for MgO and 92.0, respectively (Table 1), could have been compromised by Fe addition during

metamorphic alteration.

### 3.5. The Fox River Belt

The Fox River Belt is located in Manitoba just east of the Thompson Nickel Belt (Fig. 1), and is dated at 1882 + 1.5/−1.4 Ma (Heaman et al., 1986). It consists of two stratigraphic sequences of basalts and komatiitic basalts and two intrusions, one of which is the 2-kilometer-thick Fox River Sill (Desharnais et al., 2004). Igneous lithologies are well preserved as the grade of metamorphism is low, the prehnite-pumpellyite to the lower greenschist facies (Scoates, 1990). PRIMELT3 was run on samples containing MgO > 10%, 46 analyses provided by Desharnais et al. (2004) and 17 samples provided by Ciborowski et al. (2017). There are 11 successful primary magma solutions, yielding a mean $T_P$ = 1543 °C, similar to 1541 °C for the Chukotat group (Table 1). However, they have more highly variable MgO contents, 15.9–22.9%, yielding $T_P$ = 1457 to 1636 °C, greater than any other CSLIP member (Table 1). Given that the grade of metamorphism is low, an igneous explanation is now sought for this variability.

In Fig. 7a is shown the compositions of the basalts and komatiitic basalts together with the lithologies in Lower Central Layer Zone (LCLZ) and Upper Central Layer Zone (UCLZ) of the Fox River sill. Ignored are lithologies of the Margin Zone at the base of the sill and the Lower

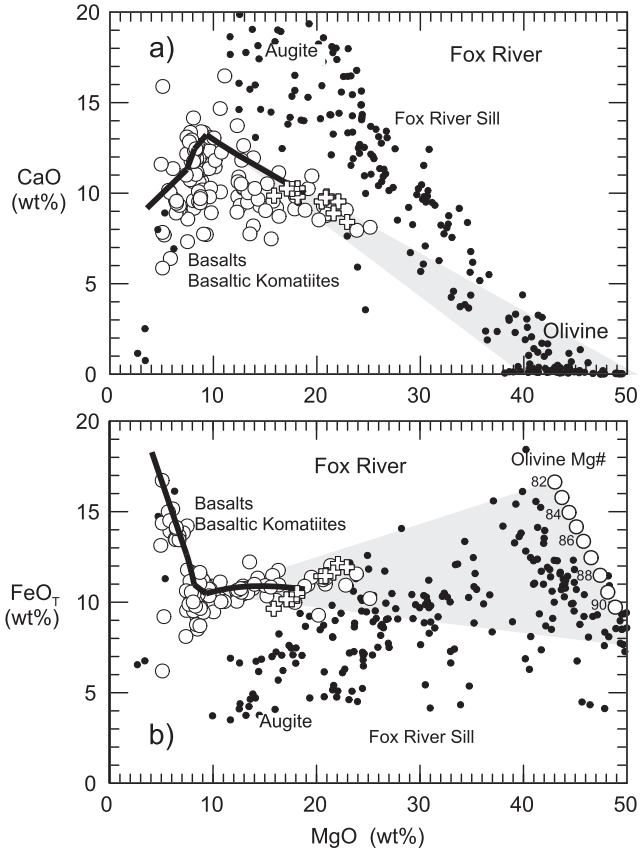


**Fig. 7.** MgO, CaO and FeO contents for rocks in the Fox River Belt (Desharnais et al., 2004) compared with model solutions. White filled circles: basalts and komatiites. Dark filled circles: intrusive igneous rocks in the Fox River sill. White crosses: PRIMELT3 primary magma solutions. Liquid line of descent is for the primary magma composition obtained from Chukotat CHK-MGO14 of Hynes and Francis (1982). Numbered circles in b) are olivine compositions having the Mg numbers shown. Gray field shows the effects of olivine addition into melts along the Ol part of the LLD. Komatiites can have a wide range of FeO contents that depend on the Mg number of olivine accumulated, yielding PRIMELT3 primary magma solutions with a wide range of MgO contents and inferred $T_P$.

Intrusion, both of which contain orthopyroxene and have been crustally contaminated (Desharnais et al., 2004). Dunite, olivine-pyroxenite and gabbro are the dominant lithologies of the sill, and these are well-described by the liquid line of descent of the primary magma of the Chukotat basalts: Ol, Ol + Cpx and OL + Cpx + Plag (Figs. 2a, 7a). Co-crystallization and possible sorting of olivine and augite are prominently displayed in the sill. And as revealed by the Chukotat basalts, many of the Fox River komatiitic basalts also have CaO contents that are lower than those described by the Ol LLD, indicating calcium loss during metamorphism.

Using the Chukotat LLD as a model, the primary magma contains 18.9% MgO and would form from the mantle at $T_P$ = 1535 °C. However, consider a whole rock composition formed by the mixing of a derivative liquid along the Ol LLD with olivine having an Mg# of ~83 (Fig. 7b). Application of PRIMELT3 will yield a successful primary magma solution with no error codes, yielding MgO = 22.9% and $T_P$ = 1636 °C. But this is an erroneous result that is ~100 °C too high. In general, PRIMELT3 can reconstruct primary magma compositions by subtraction of olivine from an olivine cumulate whole rock composition when there is similarity in the FeO contents of the olivine and liquids along the Ol LLD; for most CSLIP cases, this applies to olivines having Mg numbers of about 87 to 92 (Fig. 7b). For example, olivine accumulation does not significantly compromise solutions for Winnipegosis. However, the lesson from the Fox River case is that PRIMELT3 fails when applied to olivine cumulates having low Mg#s.

### 3.6. Molson dykes

The Molson dykes are located in the western margin of the Superior craton (Fig. 1) and are closely associated with the Thompson Nickel Belt (Heaman et al., 2009). Most were emplaced between 1885 and 1877 Ma (Heaman et al., 2009), a range that overlaps with the precise age of 1880.2 ± 1.4 for the TNB (Scoates et al., 2017). They consist of diabase, gabbro, olivine gabbro, gabbronorite, pyroxenite and coarse-grain peridotite; common minerals are clinopyroxene, olivine, orthopyroxene and primary hornblende (Scoates and Macek, 1978; Heaman et al., 2009). Whole rock analyses reveal an olivine control (Heaman et al., 2009) and, like the Fox River Belt, there is substantial heterogeneity in FeO that likely reflects cumulate mineralogical sorting. Nevertheless, Ciborowski et al. (2017) provided two PRIMELT3 solutions even though this software is applicable only for lavas. Sorting of plagioclase, augite, orthopyroxene and olivine can form cumulate rocks that may resemble liquids; successful PRIMELT3 primary magma solutions can be erroneous as will be their $T_P$ estimates.

### 3.7. Emperor volcanic complex

Ciborowski et al. (2017) reported 7 basalt compositions from the Emperor Volcanic Complex located in the Marquette Range (Fig. 1). Only one PRIMELT3 result was obtained yielding $T_P$ = 1438 °C, the lowest temperature for the CSLIP. This solution is considered untrustworthy, and it cannot be properly evaluated for a number of reasons; none of the few samples from the Emperor Volcanic Complex show an Ol LLD; the PRIMELT3 solution was obtained on sample MME08-1 which has 8.5% MgO, generally lower than liquid compositions on any Ol LLD; there is no sample description to evaluate a possible role for cumulate minerals.

### 3.8. Summary and analysis: Mantle potential temperatures for the circum-superior LIP

Fig. 8 provides a summary of 81 successful PRIMELT3 $T_P$ solutions for 425 rock compositions from the Cape Smith Belt, Roberts Lake, Winnipegosis Belt, Thompson Nickel Belt and the Fox River Belt. Of the original 86 solutions, excluded are 4 results for Winnipegosis that predict olivine Mg numbers > 92.3, higher than those measured by

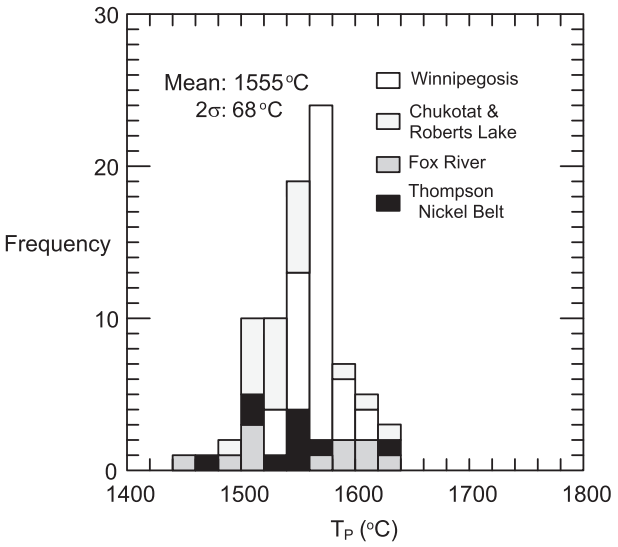


**Fig. 8.** Summary of mantle potential temperature estimates for members of the Circum-Superior Large Igneous Province. All PRIMELT3 solutions are given in Appendix A and mean values are summarized in Table 1 for each locality. Most of the variability is not a measure of true thermal variations in the mantle, but arises from metamorphic alteration and olivine addition as discussed in the text.

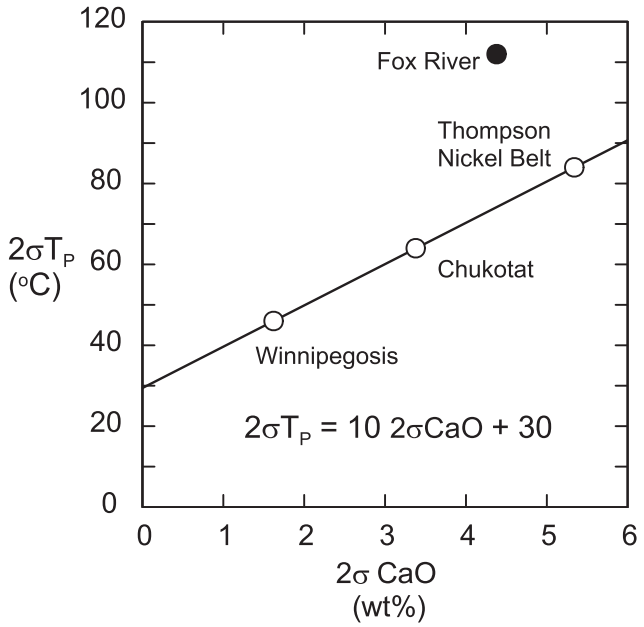


**Fig. 9.** Variations in mantle potential temperatures $T_P$ (Table 1) and CaO contents of basalts/ komatiites of members of the Circum-Superior LIP with respect to the those along the Olivine-only segment of the LLD shown in Fig. 2b and given by Eq. (4).

Waterton et al. (2017). Also excluded is the one result for the older Povungnituk basalts. The mean $T_P$ is 1555 °C and there is a 2σ variation of 68 °C. The greatest variability in $T_P$ is for the Fox River; as discussed above, the high temperature end has been compromised by whole rock accumulation of olivine having low Mg numbers. Of the 425 PRIMELT3 solutions, most are unsuccessful because they have CaO contents that are outside the bounds of primary magmas of fertile mantle peridotite. This result arises from Ca mobility during metamorphism. Evidence from the Chukotat basalts is that metamorphism also mobilized Fe, and that it compromised $T_P$. A wide range of $T_P$ solutions are obtained for samples from the Thompson Nickel Belt that experienced amphibolite facies/granulite metamorphism and intense deformation (Fig. 8). In contrast, the relatively fresh Winnipegosis komatiites exhibit the least variability in $T_P$. If Alexo komatiites are a guide (Fig. 3), there will be a ± 40 °C variation in $T_P$ stemming from ± 0.5% variations in FeO owing to metamorphic alteration.

A prediction of the hypothesis that metamorphism has contributed to $T_P$ is that its variability is correlated with a metric expected of alteration, this being variable CaO contents of the rocks with respect to the olivine LLD. The CaO contents along the Ol LLD for the primary magma of the Chukotat basalts shown in Fig. 2b is assumed to be representative of the CSLIP and is described by:

$$CaO_{Ol\ LLD} = -0.33MgO_{Ol\ LLD} + 16.18 \quad (4)$$

For each whole rock basalt/komatiite datum for the CSLIP, its CaO content is termed $CaO_{CSLIP}$ and is compared with the CaO content along the Ol LLD predicted from Eq. (4) using the mean square error as a measure of variability:

$$2\sigma CaO = 2(\Sigma(CaO_{Ol\ LLD} - CaO_{CSLIP})^2/N)^{0.5} \quad (5)$$

where N represents the number of whole rock samples in each CSLIP member; Chukotat, Winnipegosis etc. N includes all samples run with PRIMELT3, successful and unsuccessful solutions. For Winnipegosis, for example, N = 244 samples from which 44 successful PRIMELT3 solutions were obtained. There are an insufficient number of rocks from the Roberts Lake Group to work with. But for the other four members of the CSLIP, the 2σCaO are compared with the 2σ variation in $T_P$ as shown in Fig. 9. Results demonstrate that variations in mantle potential temperatures are correlated with variations in the CaO contents of basalt/komatiites, consistent with the interpretation that metamorphism has mobilized Ca together with Fe content which is coupled to primary magma MgO and $T_P$. However, it was also shown that $T_P$ can be compromised by addition of low Mg# olivine into fractionating magmas for Fox River. This may also have affected other members of the CSLIP although no evidence for it was found; additionally, Ol Mg#s for Winnipegosis (Waterton et al., 2017) are too high to have been compromised in this way. Assuming that $T_P$ estimates from basalts and komatiites from Chukotat, Winnipegosis and Thompson Nickel Belt were compromised only by metamorphism, Fig. 9 shows that:

$$2\sigma T_P = 10\ 2\sigma CaO + 30 \quad (6)$$

That is, $T_P$ varies by 10 °C for each 1 wt% CaO mobilized during metamorphism. And for perfectly fresh igneous rocks, the CSLIP variation in $T_P$ is predicted to be 30 °C. It is no coincidence that 30 °C is also the difference in $T_P$ between the mean for Winnipegosis (1572 °C) and ~1540 °C for Chukotat, Roberts Lake and Thompson Nickel Belt (Table 1).

Much of the nominal ± 68 °C variation in $T_P$ for all 81 solutions (Fig. 8) is thus demonstrated to arise from metamorphic alteration and olivine addition. It does not reflect the true thermal variability of the mantle which is 30 °C across the CLIP; added to this there is an uncertainty of ± 42 °C stemming from the PRIMELT3 algorithm (Herzberg and Asimow, 2015). It is concluded that the $T_P$ range for the CSLIP is only 30 °C and extends in space to over 1500 km from the Cape Smith Belt in the north to the Winnipegosis Belt in the southwest (Fig. 1).

There is evidence that this limited 30 °C variation in $T_P$ also occurred in time. While 1880 Ma is the commonly accepted age of the CSLIP (Heaman et al., 2009; Ciborowski et al., 2017), there exists variation: 1883.4 ± 0.8 to 1881.5 ± 0.9 Ma for Chukotat (Bleeker and Kamo, 2018; 2020); 1885 ± 2 to 1877 + 7/-4 Ma for the Molson Dyke Swarm (Heaman et al., 2009); 1870.3 ± 7.1 Ma for the Winnipegosis Belt (Waterton et al., 2017); 1870.7 ± 1.1 for the Hudson Bay Lowlands (Hamilton and Stott, 2008). These nominal ages indicate a ~12-to-15-million-year lifetime of magmatism. And at the northern margin of the Superior craton in the Cape Smith Fold Belt, the 1881.5 Ma Chukotat

Group magmatism having $T_P$ = 1541 °C was preceded by the 1998 Ma Povungnituk Group; for the later, only one sample yielded a successful solution, that being $T_P$ = 1500 °C, similar to those for the younger Chukotat basalts. More work is needed on these older basalts. Nevertheless, if the similarity is robust, it would be evidence for very little change in $T_P$ over the 116-million-year lifetime of the Cape Smith fold belt, from 1998 (Kastek et al., 2018) to 1881.5 Ma (Bleeker and Kamo, 2018).

## 4. Thermal properties of ambient mantle in the Precambrian

The constraint that there was only about a 30 °C variation in $T_P$, from ~1540 to 1570 °C for 12–15 million years, and possibly 116 million years, over thousand-kilometer distances for the Circum-Superior LIP (Fig. 1) is a characteristic of modern ambient mantle magmatism below oceanic ridges (Dalton et al., 2014) and any other plate tectonic environment removed from the influence of hotspots. The mean $T_P$ for each of the five members (Table 1) is shown again in Fig. 10 within the context of several global thermal history models. Results are similar to those reported previously (Herzberg et al., 2010) based exclusively on the Chukotat basalts. Fig. 10 shows that the results are consistent with ambient mantle thermal models characterized by sluggish mantle convection in the past (Korenaga, 2008; Herzberg et al., 2010) and with a present-day Urey ratio of about 0.38. The CSLIP temperatures in this study are higher than ambient mantle temperatures in the models of Davies (2009) and Ganne and Feng (2017), by 100 to 200 °C (Fig. 10). They are also nearly 200 °C higher than 1380 °C at 1.9 Ga suggested by Aulbach and Arndt (2019), an estimate that is similar to modern ambient mantle (Herzberg et al., 2007; Herzberg and Asimow, 2008; 2015; Matthews et al. 2021) and one that is non-unique (Herzberg, 2019). These low temperature ambient mantle models require a mantle plume origin for the basalts and komatiites from the Circum-Superior

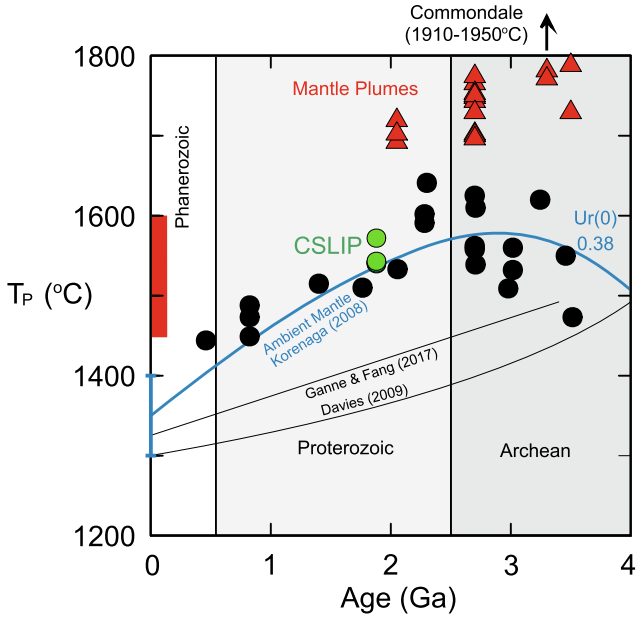


**Fig. 10.** Summary of mean $T_P$ for members of the Circum-Superior LIP (CSLIP; Table 1), high MgO komatiites from Proterozoic/Archean greenstone belts (Table 2), basalts from Phanerozoic mantle plumes (Herzberg and Asimow, 2008; 2015; Herzberg and Gazel, 2009; Jennings et al., 2019; Matthews et al., 2021) and models of ambient mantle. Mean $T_P$ for Chukotat, Roberts Lake, Thompson Nickel Belt and the Fox River Belt are all close to 1540 °C and plot on top of each other; the higher $T_P$ result, 1572 °C, is for the Winnipegosis komatiites. Solid black circles are from Herzberg et al. (2010) with age corrections from Johnson et al. (2014). Uncertainty in PRIMELT3 $T_P$ solutions is ± 42 °C (Herzberg and Asimow, 2015).

LIP and predict thermal and primary magma heterogeneity. This outcome is not consistent with the limited variability in primary magma compositions and inferred mantle potential temperatures of the CSLIP.

## 5. Thermal properties of mantle plumes in the Precambrian

A hot mantle plume origin has long been the preferred model for interpreting the high MgO contents and eruption temperatures of spinifex-textured Precambrian komatiites (Jarvis and Campbell, 1983; Herzberg, 1992; Nisbet et al., 1993; Arndt et al., 2008; Puchtel et al., 2022). It must also satisfy the requirement that its thermal state be hotter than that of ambient mantle (Nisbet et al., 1993; Herzberg, 1995; Herzberg et al., 2007; 2010). However, in the early Earth, ambient mantle was also hot owing to increased radiogenic heat production (Davies, 1980; Richter, 1985; Christensen, 1985; Korenaga, 2008). Therefore, how can we distinguish the melt products of hot ambient mantle from those of a hot mantle plume?

Petrological models of modern mantle plumes constrain them to have $T_P$ in excess of ambient mantle by 100–250 °C (Fig. 10; Herzberg and Asimow, 2008; 2015; Herzberg and Gazel, 2009; Jennings et al., 2019; Matthews et al., 2021). Their magmatic products have no diagnostic set of geochemical properties and could have formed by the melting of depleted, primitive, and enriched mantle sources (e.g., Kerr et al., 1995). The benchmark is that $T_P$ for ambient mantle be known, and this can be constrained from petrology to be about 1350 °C at the present time from work on olivine phyric basalts from the Siqueiros Fracture Zone, representative of the East Pacific Rise spreading center in that area (Herzberg and Asimow, 2015; Matthews et al., 2021). According to Dalton et al. (2014), temperatures vary by 30 °C over oceanic ridge lengths similar in dimensions to the periphery of the Superior craton. But in deep Earth time, this tectonic constraint does not exist. Therefore, the identification of mantle plumes in the Precambrian must satisfy the requirement that their primary magmas were hotter than those produced from ambient mantle at the time.

An examination is now made of the thermal properties of the mantle sources for well-studied komatiite occurrences from the Lapland, Abitibi, Barberton, and Commondale greenstone belts. The method used to solve the primary magma problem was discussed in Section 2.2. A determination is made of the melt composition in equilibrium with an observed olivine having the highest Mg#. Primary magma MgO contents are either as reported in the literature or calculated by application of the Olivine Calculator in PRIMELT3 on whole rock samples. Olivine liquidus and mantle potential temperatures were then obtained from primary magma MgO contents from Eqs. (1) and (2) (Herzberg and Asimow, 2015). Results are given in Table 2 and shown in Fig. 10.

### 5.1. Lapland greenstone belt

Paleoproterozoic komatiites and picrites of Lapland Greenstone Belt are part of a belt that continues 400 km to northern Norway (Hanski et al., 2001), and the most thoroughly studied locations are from Jeesiörova and Kevitsa (Hanski et al., 2001; Puchtel et al., 2020) in Finland. Ages for Jeesiörova and Kevitsa are 2049 ± 13 Ma (Puchtel et al., 2020), similar to 2056 ± 25 Ma for Jeesiörova (Hanski et al., 2001). All volcanic rocks have been metamorphosed in the greenschist to epidote amphibolite facies. Olivine is only preserved the Kevitsa dikes and it has a maximum Mg# of 94.1 (Puchtel et al., 2020).

Puchtel et al. (2020) calculated MgO contents of 25.2 to 26.3% using the method of incremental addition of olivine into a selected komatiite composition, KD-14, until it was in equilibrium with olivine having the highest observed Mg#, 94.1. Using the PRIMELT3 Olivine Calculator for KD-14 yields a melt composition with 25.6% MgO that is in equilibrium with olivine Mg# of 94.1 (Table 2). Application of Eq. (2) yields $T_P$ ~ 1700 °C for the Lapland komatiites, about 150 °C higher than the mean CSLIP (Fig. 10).

**Table 2**
Komatiite Primary Magma MgO Contents and Mantle Potential Temperatures.

| Location | Age (Ga) | Source/Method | $K_D$ | $FeO/FeO_T$ | Ol Mg# (max) | MgO (wt%) | TOl (°C) eq (1) | $H_2O$ (wt%) | $T_P$ (°C) eq (2) or (3) |
|---|---|---|---|---|---|---|---|---|---|
| Lapland | 2.05 | Puchtel et al. (2020) | | | 94.1 | 25.2* | 1533 | 0 | 1692 |
| Lapland | 2.05 | Puchtel et al. (2020) | | | 94.1 | 26.3* | 1550 | 0 | 1719 |
| Lapland | 2.05 | Ol Calculator on Puchtel et al. (2020) | 0.29 | 0.92 | 94.1 | 25.6 | 1539 | 0 | 1702 |
| Belingwe | 2.7 | Asafov et al. (2018) | 0.32 | 0.92 | 93.5 | 27.5* | 1569 | 0 | 1748 |
| Belingwe | 2.7 | Asafov et al. (2018) | 0.32 | 0.92 | 93.5 | 27.5* | 1563 | 0.2 | 1743 |
| Belingwe | 2.7 | Nisbet et al. (1993) | 0.30 | 0.89 | 93.6 | 25.6* | 1539 | 0 | 1702 |
| Belingwe | 2.7 | Ol Calculator on Puchtel et al. (2009) | 0.30 | 0.89 | 93.6 | 25.5 | 1538 | 0 | 1700 |
| Belingwe | 2.7 | Ol Calculator on Puchtel et al. (2009) | 0.30 | 0.89 | 93.6 | 25.5 | 1532 | 0.2 | 1696 |
| Alexo | 2.7 | Arndt (1986) | 0.30 | 0.95 | 94.1 | 28.2* | 1580 | 0 | 1765 |
| Pyke Hill | 2.7 | Sobolev et al. (2016) | 0.30 | 0.90 | 94.5 | 28.6* | 1586 | 0 | 1774 |
| Pyke Hill | 2.7 | Sobolev et al. (2016) | 0.30 | 0.90 | 94.5 | 28.6* | 1569 | 0.6 | 1753 |
| Pyke Hill | 2.7 | Ol Calculator on Puchtel et al. (2009) | 0.29 | 0.90 | 94.5 | 27.6 | 1571 | 0 | 1750 |
| Pyke Hill | 2.7 | Ol Calculator on Puchtel et al. (2009) | 0.29 | 0.90 | 94.5 | 27.6 | 1554 | 0.6 | 1729 |
| Barberton ADK | 3.48 | Ol Calculator on Puchtel et al. (2013) | 0.30 | 0.90 | 93.4 | 26.7 | 1557 | 0 | 1729 |
| Barberton AUK | 3.48 | Ol Calculator on Parman et al. (2004) | 0.29 | 0.90 | 93.9 | 29.2 | 1595 | 0 | 1788 |
| Barberton AEK | 3.3 | Ol Calculator on Connolly et al. (2011) | 0.30 | 0.90 | 95.1 | 28.9 | 1655 | 0 | 1781 |
| Barberton AEK | 3.3 | Ol Calculator on Connolly et al. (2011) | 0.30 | 0.90 | 95.1 | 28.9 | 1646 | 0.28 | 1771 |
| Commondale | 3.33 | Wilson (2019) | 0.33 | 0.87 | 96.6 | 36.1* | 1691 | 0 | 1948 |
| Commondale | 3.33 | Ol Calculator on Wilson (2019) | 0.29 | 0.90 | 96.6 | 34.4 | 1669 | 0 | 1909 |

* MgO contents as reported; T Ol, olivine liquidus temperature at 1 atmosphere; $T_P$, mantle potential temperature.

### 5.2. Belingwe greenstone belt

The 2.7 Ga komatiites from the Reliance Formation of the Belingwe Greenstone Belt are variably altered and with olivine phenocrysts preserved (Nisbet et al. 1993). Using the Olivine Calculator in PRIMELT3 on samples from Puchtel et al. (2009) yields 25.5% MgO for primary magmas in equilibrium with olivine having an Mg# of 93.5 (Table 2). This result agrees well with chill compositions having 25.6% MgO and containing olivine phenocrysts with an Mg# of 93.6 (Nisbet et al. 1993).

Asafov et al. (2018) determined the Belingwe primary magma with 27.5% MgO was in equilibrium with olivine having an Mg# of 93.5. This calculation was based on the reconstruction of low MgO melt inclusions trapped in olivine using $K_D = 0.32$ and $FeO/FeO_T = 0.92$. Asafov et al. (2018) also determined the primary magma contained 0.2% $H_2O$; this amount of water has a negligible effect on lowering olivine liquidus and mantle potential temperatures (Table 2), based on the calibration of Rhyolite-MELTS at QFM-1 and 250 bars (Gualda et al., 2012). Relative to ambient mantle with a Urey ratio of ~0.38 as constrained by the CSLIP, $T_P$ for the Belingwe mantle plume was hotter by about 100–150 °C (Fig. 10).

### 5.3. Abitibi greenstone belt

Arndt (1986) reported a maximum olivine Mg number of 94.1 in the 2.7 Ga komatiites at Alexo and calculated 28.2% in the primary magma. (Sobolev et al., 2016) reported a maximum of 94.5 and an olivine grain with this Mg# was found to host a reconstructed melt inclusion having 28.6% MgO (Sobolev et al., 2016), very similar to the Arndt determination. The volatile-free olivine liquidus $T_1^{Ol/L}$ and mantle potential $T_P$ temperatures in the melt inclusion study are 1586° and 1774 °C from Eqs. (1) and (2) (Herzberg and Asimow, 2015). But dissolved $H_2O$ will lower these temperatures. Sobolev et al. (2016) used a calibration by Falloon and Danyushevsky (2000) to suggest that $T_1^{Ol/L}$ would decrease by 60 °C owing to their measured 0.6% $H_2O$ in the primary magma. However, there exist other calibrations and these yield a lower temperature drop:

- 9 °C (Sugawara 2000)
- 23 °C (Medard and Grove, 2008; Ueki et al., 2020)
- 17 °C (Rhyolite-MELTS at QFM-1 and 250 bars; Gualda et al., 2012).

Making use of Eq. (3) shows that the Falloon and Danyushevsky (2000) calibration would propagate to a lowering of $T_P$ from 1774 to 1687 °C, a significant decrease of 87 °C. Using MELTS and Eq. (3) yields decrease in $T_P$ of only ~21 °C with 0.6% $H_2O$ (Table 2), a result that is used here.

As an independent test, the Olivine Calculator in PRIMELT3 was applied to komatiites from Pyke Hill reported by Puchtel et al. (2009). Results show that olivine with an Mg# of 94.5 would have been in equilibrium with a primary magma having 27.6% MgO, in good agreement with 28.2% and 28.6% MgO in the determinations by Arndt (1986) and Sobolev et al. (2016), respectively. Relative to ambient mantle with a Urey ratio of ~0.38 as constrained by the CSLIP, $T_P$ for the Abitibi mantle plume was hotter by 150 to 200 °C (Fig. 10).

### 5.4. Barberton greenstone belt

There are three komatiite types from the Barberton Greenstone Belt to consider. Those in the type locality of the Komati Formation were emplaced at 3.48 Ga (Blichert-Toft et al., 2015) and are depleted in alumina (UDK type) owing to separation from residual garnet (Herzberg, 1992; Robin-Popieul et al., 2012). Slightly younger are komatiites from the Hooggenoeg Formation, which are alumina-undepleted (AUK type) indicating separation from residual harzburgite or dunite (Herzberg, 1992; Robin-Popieul et al., 2012), similar to komatiites from the Abitibi Greenstone Belt. Younger still are the 3.3 Ga komatiites from the Weltevreden Formation, enriched in alumina and depleted in titanium (AEK type), and which separated from a highly refractory residue (Robin-Popieul et al., 2012).

The primary magma composition for komatiites from the Komati Formation was estimated from whole rock compositions reported by Puchtel et al. (2013) and their olivine having the highest Mg#, which is 93.4. Using the Olivine Calculator in PRIMELT3 and assuming $FeO/FeO_T = 0.90$, the primary magma has 26.7% MgO and $K_D$ is 0.30 (Table 2), similar to 27% MgO estimated by Robin-Popieul et al. (2012). In contrast, Puchtel et al. (2013) and Nicklas et al. (2019) obtained 29.4% MgO, higher only because they assumed $FeO = FeO_T$ rather than $FeO = 0.9FeO_T$ in this work (Table 2). Chill margins contain 25.3–29.4% MgO (Puchtel et al., 2013); while they are assumed to represent quenched liquids, 12% addition of cumulate olivine can raise MgO from 26.7 to 29.4%.

Parman et al. (2004) reported chill margin compositions at the Horizon 1 section of the Komati Formation, which have the properties of AUK from the above Hooggenoeg Formation; olivine has 93.9 as the highest Mg#. Using the Olivine Calculator in PRIMELT3 and assuming $FeO/FeO_T = 0.90$, the primary magma has 29.2% MgO (Table 2), similar

to 30% MgO estimated by Robin-Popieul et al. (2012) for the Hooggenoeg Formation.

The primary magma problem was solved for komatiites from the Weltevreden Formation using whole rock data from Connolly et al. (2011) and their reported maximum Mg# for olivine, which is 95.1. The MgO content is 28.9% (Table 2), nearly identical to the result for AUK from the Komati Formation, but lower than 33% estimated by Robin-Popieul et al. (2012). Puchtel et al. (2013) and Nicklas et al (2019) obtained 31.4 ± 0.9% MgO higher than 28.9% in this work only because they assumed FeO = $FeO_T$ rather than FeO = 0.9$FeO_T$ (Table 2). Sobolev et al. (2019) reported 0.28% $H_2O$ in olivine-hosted melt inclusions, an amount that will have an insignificant effect on mantle potential temperature.

In summary, primary magma compositions from the Barberton Greenstone belt are lowest for the ADK, 26.7%, increasing to ~29% for AUK and AEK types. Using Eq. (2), calculated $T_P$ ranges from 1729 to 1788 °C (Table 2). This variation is characteristic of the tapping of primary magmas from a thermally heterogeneous mantle plume, cooler in the garnet-bearing periphery (ADK) and hotter in the axis containing residual harzburgite or dunite (AUK). These mantle potential temperatures are also about 200 °C higher than ambient mantle with a Urey ratio of ~0.38 as constrained by the CSLIP (Fig. 10).

### 5.5. Commondale greenstone belt

Wilson (2019) provided an authoritative documentation of komatiites from the Commondale Greenstone Belt, and I will work exclusively with this information. They are located 50 km from the Barberton Greenstone Belt, and its komatiites are slightly younger, 3.3 Ga. The komatiites are highly depleted in all lithophile trace elements, and they are classified as alumina-enriched komatiites. They have the lowest $FeO_T$ contents on record and were likely formed as partial melts of a highly refractory residue (Wilson, 2019). They contain olivines with a maximum Mg# of 96.6, the highest worldwide. Wilson (2019) estimated 36.1% MgO in the primary magma using $K_D$ = 0.33; using the Olivine Calculator in PRIMELT3 lowers this to 34.4% MgO with $K_D$ = 0.29. $T_P$ is 1909 and 1948 °C for both cases (Table 2), potentially the hottest komatiites ever to have erupted (Wilson, 2019), a result that plots off the scale in Fig. 10. However, Wilson and Bolhar (2021) provided evidence that the Commondale komatiites may have contained water from the mantle transition zone and, if confirmed, the mantle potential temperature may have been lower.

### 5.6. Summary for Precambrian mantle plumes

Komatiites from the Lapland, Abitibi, and Barberton greenstone belts formed from sources that had mantle potential temperatures that were 100–200 °C higher than that of ambient mantle as represented by the Circum-Superior LIP and the Korenaga (2008) model with a Urey ratio of ~0.38 (Fig. 10). This temperature difference, or excess, is similar to 100–250 °C of Phanerozoic mantle plumes (Herzberg and Asimow, 2008; 2015; Herzberg and Gazel, 2009; Jennings et al., 2019; Matthews et al., 2021), demonstrating approximate constancy of thermal properties of mantle plume structures through time.

An alternate interpretation is that the high MgO komatiites formed in the hot axis of a mantle plume, and the basalts/ low MgO komatiites from the CSLIP formed in the plume head that was cooler owing to entrainment of ambient mantle (Campbell et al., 1989; Campbell and Griffiths, 1990; Barnes et al., 2021). However, there is no evidence for entrainment from numerical modeling and geochemistry (Farnetani and Samuel, 2005; Sleep, 2008). And petrological modelling indicates just the opposite; many Phanerozoic basalts that erupted initially from plume heads were hotter than those that later erupted from plume axes (Herzberg and Gazel, 2009; Trela et al., 2015).

Of the Precambrian high MgO komatiites considered in Fig. 10, the Commondale komatiites are a notable high temperature outlier, with an excess temperature of about 350 °C. A notable outlier in the Phanerozoic is the Cretaceous age Tortugal lavas of Costa Rica, related to the ancestral Galapagos mantle plume (Trela et al., 2017); olivines have a maximum Mg# of 94.2 and crystallized from high MgO melts with spinel at 1570 °C as constrained by the Al-in-Olivine thermometer; use of Eq. (3) yields $T_P$ = 1754 °C, about 400 °C higher than ambient mantle at that time, and significantly hotter than any other Phanerozoic mantle plume. With these ancient and modern outliers in mind, the results of this study indicate that most Precambrian mantle plumes were 100 to 200 °C hotter than the ambient mantle reference frame as defined by the Korenaga (2008) model with a present-day Urey ratio of ~0.38, similar to 100–250 °C for Phanerozoic mantle plumes (Fig. 10).

## 6. The mantle plume model for the circum-superior LIP

The most popular model for the CSLIP is that it formed in a mantle plume (Ernst and Bleeker, 2010; Ernst and Buchan 2004; Minifie et al., 2013; Ciborowski et al, 2017; Waterton et al., 2017; Kastek et al., 2020; Bleeker and Kamo, 2020; Barnes et al., 2021; Condie et al., 2021). Based on the work of Sleep et al. (2002), Ciborowski et al. (2017), Waterton et al. (2017), Kastek et al. (2018) and Bleeker and Kamo (2020) proposed that a mantle plume impacted the base of the thick Superior craton, it flowed up and laterally, and melted around the margins where the craton was thinned previously. The essential problem for the mantle plume model for the CLIP is that it predicts thermal heterogeneity, in contrast with the evidence presented here that $T_P$ remained little changed at ~1540–1570 °C for 12–15 million years, and possibly 116 million years, of CSLIP magmatism.

Petrological modelling indicates that $T_P$ for Phanerozoic mantle plumes is in excess of ambient mantle by 100–250 °C (Fig. 10; Herzberg and Asimow, 2008; 2015; Herzberg and Gazel, 2009; Jennings et al., 2019; Matthews et al., 2021), dropping to ambient mantle temperatures at the peripheries (Sleep, 2008; Farnetani and Samuel, 2005). This is consistent with Sleep's (2008) model of a ~100 to 300 °C temperature variability from the hot interior to the cooler periphery. It is also consistent with petrological models that show a 100 °C variability in $T_P$ for basalts sampled from individual mantle plume occurrences (e.g., Galapagos; Herzberg and Gazel, 2009). Similarly, Al-in-olivine thermometry for high Mg# olivines reveals a ~100 °C variability for both the Paraná–Etendeka mantle plume (Jennings et al., 2019) and the ancestral Icelandic plume that produced the Paleocene picrites at Baffin Island and West Greenland (Spice et al., 2016). Primary magmas that are tapped from a thermally heterogenous mantle plume must have variable MgO contents, in contrast with those of the Circum-Superior LIP (Table 1).

Another source of thermal heterogeneity can arise when a plume impacts the base of the lithosphere. Its high temperatures can yield melts with high $T_P$ for millions of years, but only if the plume head is continuously supplied by its conduit (Sleep, 2008). However, 3-D models of Sleep (2008) indicate a plume head can cool by 100 °C in about 2 million years owing to heat loss to the lithosphere should it rise as a blob not connected to a conduit. Rapid cooling is also expected as the lithosphere moves independently of the conduit, yielding an initial flood basalt stage followed by a hot spot track as in the modern Earth (Richards et al., 1989). There is a substantial body of evidence that rapid cooling of mantle plumes was responsible for the production of Phanerozoic LIPS of short duration.

Unlike the Paleoproterozoic Circum-Superior LIP, the main phase of volcanism for all major Phanerozoic continental LIPS was less than 1 million years. Examples are the Central Atlantic Igneous Province (CAMP; Blackburn et al., 2013; Davies et al., 2021), the Siberian Traps (Kamo et al., 2003; Burgess et al., 2017), the Emeishan Traps (Xu et al., 2018), the Karoo LIP (Svensen et al., 2012), the Columbia River basalt (Kasbohm and Schoene, 2018; Black et al., 2021), and the Deccan Traps (Sprain et al., 2019; Schoene et al., 2019). Exceptions are longer eruptions for the Paraná–Etendeka LIP (3 Ma; Gomes and Vasconcelos, 2021)

and the North Atlantic Igneous Province (NAIP; Larsen et al., 2016). At the West Greenland part of the NAIP, where the chronostratigraphy is well-constrained, eruption rates were greatest between 62 and 60 Ma, and declined during the following 6 million years (Larsen et al., 2016). These short lifetimes are consistent with rapid cooling associated with lithospheric plates that moved independently of their conduits or mantle plumes that were mostly heads that separated from their tails (Sleep, 2008). In contrast, the relative longevity of the 12–15 million years of the CSLIP would require a fixed coupling of the mantle conduit to the Superior cratonic lithosphere. It is difficult to imagine how a thermally heterogenous mantle plume could lock on and impact the base of the Superior craton, cool down as it flowed outwards at thousand-kilometer distances and melt to produce primary magmas that were all so similar, with 19–20% MgO (Table 1). A single mantle plume origin for the CSLIP (Ernst and Bleeker, 2010; Minifie et al., 2013; Ciborowski et al, 2017; Bleeker and Kamo, 2020) is without a Phanerozoic analog.

## 7. A plate tectonic model for the circum-superior LIP

Fig. 11 is a plate tectonic model for the CSLIP where ambient mantle melting could have occurred by passive upwelling of asthenosphere below continental rifts contemporaneously with plate convergence (Heaman et al., 2009; Corrigan et al., 2009; Percival et al., 2005). It is based on a geodynamic model of Chowdhury et al. (2020) at $T_P$ = 1525 °C. At these high mantle temperatures, the asthenosphere mantle viscosity is low and the angle of subduction is steep. This results in slab roll-back, retreat of the subduction trench, extension and thinning of the overriding continental lithospheric plate and its replacement with hot upwelling ambient asthenosphere mantle. In this model, partial melts yielded basalts and komatiites in both the Manikewan oceanic crust and continental rifts at the periphery of the Superior craton. The initial stage of lithosphere extension and asthenosphere upwelling is expected to have led to a close spatial association of melts from the cold subducted lithosphere and those from the hot asthenosphere. This is a plausible explanation for the penecontemporaneous relationship between the ~1880 Ma Molson Dykes, Fox River, and Winnipegosis and continental arc type calc-alkaline plutons in the Fin Flon - Thompson Nickel Belt (Corrigan et al., 2009; Percival et al., 2005).

The period between ~2.1 and 1.8 Ga corresponds with the world-wide formation of collisional orogenic belts (e.g. Zhao et al., 2002; French et al., 2008; Wan et al., 2020; Condie et al., 2021), which sutured together cratons during the assembly of the supercontinent Nuna/Columbia (Wan et al., 2020). French et al. (2008) reviewed the evidence that during this period of global crustal amalgamation, mafic/ultramafic intraplate and plate margin magmatism occurred in association with crustal extension/transtension. The tectonics is very different from Phanerozoic mantle plumes that produced the NAIP, Karoo, Paraná–Etendeka, and possibly CAMP large igneous provinces; for these, mantle plumes were associated in space and time with continental rifting, breakup, and seafloor spreading (e.g., Coffin and Eldholm, 1994; Storey, 1995; Courtillot et al., 1999; Saunders et al., 1997; Buiter and Torsvik, 2014; Larsen and Williamson, 2020; Condie et al., 2021). While LIPS such as the Ontong Java Plateau may be associated with subduction by accretion (Petterson et al., 1999), this is not the model of Ciborowski et al. (2017), Waterton et al. (2017), and Bleeker and Kamo (2020). Although the association of the CSLIP with collisional rather than breakup tectonics is insufficient evidence to falsify the mantle plume model, it is notable that there is no Phanerozoic analog.

Delamination is another process wherein zones of subcontinental lithospheric mantle can be replaced by upwelling hot asthenosphere (Göğüş and Ueda, 2018; Chowdhury et al., 2020). It could have occurred by the peeling off of subcontinental lithospheric mantle in the downgoing slab, exposing the overriding and thickened continental crust to heat from the hot upwelling asthenosphere. Delamination could explain the ultrahigh temperature metamorphism of the Trans-Hudson Orogen (Spencer et al., 2021). And ambient mantle potential temperatures remained high throughout the mid-Proterozoic (Fig. 10), which may explain why hot orogenesis continued during this time (Spencer et al., 2021).

It is concluded that the upwelling of hot ambient asthenosphere mantle by lithosphere extension and/or delamination in a plate tectonic model was important in the Paleoproterozoic. It can link production of high Mg basalts and komatiites in the Circum-Superior LIP with hot ambient mantle magmatism, collisional tectonics, the closure of the Manikewan Ocean, and formation of the hot Trans-Hudson Orogen of Laurentia (Corrigan et al., 2009).

## 8. Discussion and conclusions

Implementation of PRIMELT3 software (Herzberg and Asimow, 2015) on a large database of basalts and komatiites from the Circum-Superior Large Igneous Province reveals limited variability in primary magma composition and inferred mantle potential temperature (Fig. 8; Table 1). Most of the variability is demonstrated to arise from Fe mobility during metamorphism and olivine addition into differentiated magmas. For volcanic rocks from the Cape Smith Belt, Roberts Lake, Thompson Nickel Belt, and the Fox River Belt, the mean MgO content is 19.1% and the mean $T_P$ is 1541 °C; Winnipegosis komatiite means are slightly higher, 20.3% MgO and 1572 °C. The $T_P$ range for the CSLIP was therefore only about 30 °C, highly uniform over ~12 to 15 million years in time and over 1500 km in space from the Cape Smith Belt in the north to the Winnipegosis Belt in the southwest (Fig. 1). This limited long

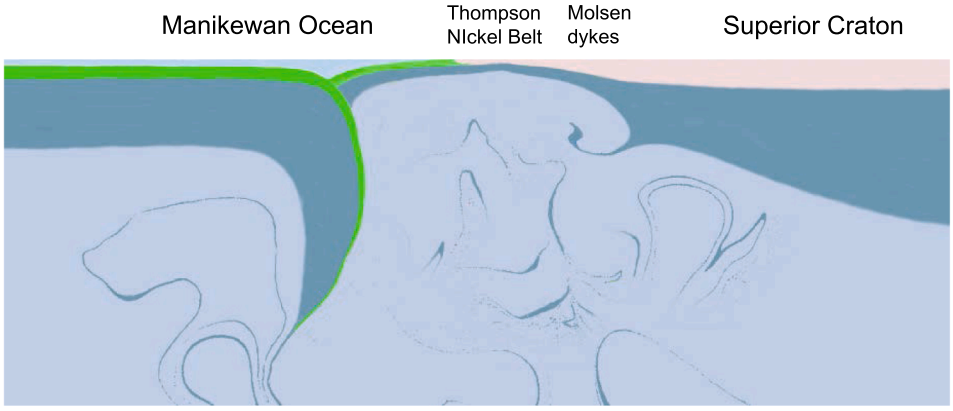


**Fig. 11.** A plate tectonic model for the Circum-Superior Large Igneous Province, modified from a simulation at $T_P$ = 1525 °C from Chowdhury et al. (2020). Similar plate tectonic models were proposed earlier by Percival et al. (2005) and Corrigan et al. (2009) to account for the close association of mafic/ultramafic rocks of the CSLIP with arc type calc-alkaline plutons in the Fin Flon - Thompson Nickel Belt area.

wavelength variation in $T_P$ is characteristic of modern ambient mantle magmatism below oceanic ridges and any other plate tectonic environment removed from the influence of hotspots, not mantle plumes.

The ambient mantle melting model predicts limited primary magma temperature and composition variations elsewhere in the CSLIP not considered here (e.g., Labrador Trough), and more work would be welcomed. Moreover, there is similarity between one $T_P$ result for a basalt from the much older 1998 Ma Povungnituk Group and those for the 1882 Ma Chukotat Group of the Cape Smith Belt, indicating thermal homogeneity over a 116 Ma lifetime The implication is that all basalts and komatiites from the greater Circum-Superior Belt with ages spanning the full ~1880 to 2100 Ma range (Heaman et al., 2009) may have originated by ambient mantle melting, and the CSLIP may have been a late-stage part of a magmatic continuum that started hundreds of millions of years earlier; however, more work is needed before this conclusion is secure.

Basalts and low MgO komatiites from the Circum-Superior LIP provide an important ambient mantle temperature reference frame for understanding high MgO komatiites that formed in Precambrian mantle plumes. A critical evaluation of high MgO komatiites from the Lapland, Abitibi, and Barberton greenstone belts shows that they formed from sources that had mantle potential temperatures that were 100–200 °C higher than those of ambient mantle as represented by the Circum-Superior LIP and the Korenaga (2008) model with a Urey ratio of ~0.38 (Fig. 10). This temperature difference, or excess, is similar to that of Phanerozoic mantle plumes, indicating that most mantle plumes throughout Earth history have been about 100 to 250 °C hotter than ambient mantle.

Modern mantle plumes differ from ambient mantle in displaying spatial heterogeneity in temperature, with plume heads and conduits that can be 100–250 °C higher than their ambient mantle periphery. In time, mantle plume heads that impact the base of the lithosphere can cool rapidly owing to heat loss to the lithosphere. Rapid cooling explains why the main phase of volcanism for most major Phanerozoic continental LIPS produced by mantle plumes took place in a time frame of under 1 million years. Thermal heterogeneity yields heterogeneous primary magmas having a range of MgO contents. It is therefore difficult to understand how a thermally heterogeneous mantle plume for the Circum-Superior LIP could have impacted the base of the Superior craton, cool down as it flowed outwards at thousand-kilometer distances and melted to produce primary magmas that were all so similar, with 19–20% MgO during its 12–15-million-year lifetime. And the Circum-Superior LIP differs from modern LIPS wherein mantle plume magmatism is associated in space and time with continental rifting, breakup, and seafloor spreading. There is no Phanerozoic mantle plume analog model for the CSLIP.

Uniformity of primary magma compositions and mantle potential temperatures inferred for basalts and komatiites from the Circum-Superior LIP are consistent with ambient mantle melting below continental rifts in a plate tectonic model as suggested in the pioneering studies of Heaman et al. (2009), Corrigan et al. (2009) and Percival et al. (2005). Ambient mantle melting could have occurred during slab rollback, retreat of the subduction trench, extension and thinning of the overriding continental lithospheric plate and its replacement with hot upwelling asthenosphere mantle (Fig. 11). Partial melts yielded basalts and komatiites in both the Manikewan oceanic crust and continental rifts at the periphery of the Superior craton. The plate tectonic model associates the Circum-Superior LIP with collisional rather than breakup tectonics, closure of the Manikewan Ocean, formation of the Trans-Hudson Orogen of Laurentia (Corrigan et al., 2009), and the worldwide suturing of other cratons during assembly of the supercontinent of Nuna/Columbia about 1.9 billion years ago (e.g., Zhao et al., 2002; French et al., 2008; Wan et al., 2020; Condie et al., 2021).

Understanding the association of LIPS with supercontinent breakup in the Phanerozoic and assembly in the Paleoproterozoic has proven puzzling (Ernst and Bleeker, 2010; Condie et al., 2021). The results of this study on the Circum-Superior LIP indicate that progress might be made by relaxing the commonly held assumption or expectation that all or most Precambrian LIPS were produced by mantle plumes.

## Funding

This research was not supported any grant from any funding agency in the public, commercial, or not-for-profit sectors.

## CRediT authorship contribution statement

**Claude Herzberg:** Conceptualization, Data curation, Formal analysis, Methodology, Project administration, and Writing.

## Declaration of Competing Interest

The authors declare that they have no known competing financial interests or personal relationships that could have appeared to influence the work reported in this paper.

## Acknowledgements

The author is grateful to Michael Lesher, Larry Heaman, Priyadarshi Chowdhury and Jun Korenaga for helpful and stimulating comments and to Andrew Kerr for providing a map of the CSLIP. I am very grateful to Igor Puchtel and an anonymous reviewer for their thoughtful and thorough reviews.

## Appendix A. Supplementary material

Whole rock compositions and their PRIMELT3 primary magma solutions are listed in Appendix A. Supplementary data to this article can be found online at https://doi.org/10.1016/j.precamres.2022.106671.

## References

Agee, B.C., Walker, D., 1990. Aluminum partitioning between olivine and ultrabasic 205 silicate liquid to 6 GPa. Contrib. Mineral. Petrol. 105, 243–254.
Ahern, J.L., Turcotte, D.L., 1979. Magma migration beneath an ocean ridge. Earth Planet. Sci. Lett. 45 (1), 115–122.
Arndt, N.T., 1986. Differentiation of komatiites flows. J. Petrol. 27, 279–301.
Arndt, N.T., Lesher, C.M., Barnes, S.J., 2008. Komatiite. Cambridge University Press, p. 467.
Asafov, E.V., Sobolev, A.V., Gurenko, A.A., Arndt, N.T., Batanova, V.G., Portnyagin, M. V., Garbe-Schönberg, D., Krasheninnikov, S.P., 2018. Belingwe komatiites (2.7 Ga) originate from a plume with moderate water content, as inferred from inclusions in olivine. Chem. Geol. 478, 39–59.
Aulbach, S., Arndt, N.T., 2019. Eclogites as paleodynamic archives: Evidence for warm (not hot) and depleted (but heterogeneous) Archaean ambient mantle. Earth Planet. Sci. Lett. 505, 162–172.
Baragar, W.R.A., Scoates, R.F.J., 1981. The Circum-Superior Belt; a Proterozoic plate margin? In: Kroener, A. (Ed.), Precambrian Plate Tectonics. Elsevier, Amsterdam, pp. 297–330.
Barnes, S.J., Williams, M., Smithies, R.H., Hanski, E., Lowrey, J.R., 2021. Trace Element Contents of Mantle-Derived Magmas Through Time. J. Petrol. 62 https://doi.org/10.1093/petrology/egab024.
Beattie, P., 1993. Olivine-melt and orthopyroxene-melt equilibria. Contrib. Mineral. Petrol. 115, 103–111.
Berry, A.J., Stewart, G.A., O'Neill, H.S., Mallmann, G., Mosselmans, J.F.W., 2018. A re-assessment of the oxidation state of iron in morb glasses. Earth Planet. Sci. Lett. 483, 114–123. https://doi.org/10.1016/j.epsl.2017.11.032.
Bézos, A., Guivel, C., La, C., Fougeroux, T., Humler, E., 2021. Unraveling the confusion over the iron oxidation state in MORB glasses. Geochim. Cosmochim. Acta 293, 28–39.
Black, B.A., Karlstrom, L., Mather, T.A., 2021. The life cycle of large igneous provinces. Nature Rev. 2 (12), 840–857. https://doi.org/10.1038/s43017-021-00221-4.
Blackburn, T.J., Olsen, P.E., Bowring, S.A., McLean, N.M., Kent, D.V., Puffer, J., McHone, G., Rasbury, E.T., Et-Touhami, M., 2013. Zircon U-Pb Geochronology Links the End-Triassic Extinction with the Central Atlantic Magmatic Province. Science 340 (6135), 941–945.
Bleeker, W., Kamo, S.L., 2018. Extent, origin, and deposit-scale controls of the 1883 Ma Circum-Superior large igneous province, northern Manitoba, Ontario, Quebec, Nunavut and Labrador. In: Rogers, N. (Ed.), Targeted Geoscience Initiative: 2017 Report of Activities. Geological Survey of Canada, Open File 8373 vol 2, pp. 5–14.

Bleeker, W., Kamo, S., 2020. Structural-stratigraphic setting and U-Pb geochronology of Ni-Cu-Co-PGE ore environments in the central Cape Smith Belt, Circum-Superior Belt; *in* Targeted Geoscience Initiative 5: Advances in the understanding of Canadian Ni-Cu-PGE and Cr ore systems – Examples from the Midcontinent Rift, the Circum-Superior Belt, the Archean Superior Province, and Cordilleran Alaskan-type intrusions, (Ed.) W. Bleeker and M.G. Houle; Geological Survey of Canada, Open File 8722, 65–98. https://doi.org/10.4095/326882.

Blichert-Toft, J., Arndt, N.T., Wilson, A., Coetzee, G., 2015. Hf and Nd isotope systematics of early Archean komatiites from surface sampling and ICDP drilling in the Barberton Greenstone Belt, South Africa. Am. Mineral. 100 (11–12), 2396–2411.

Buiter, S.J.H., Torsvik, T.H., 2014. A review of Wilson Cycle plate margins: A role for mantle plumes in continental break-up along sutures? Gondwana Res. 26 (2), 627–653.

Burgess, S.D., Muirhead, J.D., Bowring, S.A., 2017. Initial pulse of Siberian Traps sills as the trigger of the end-Permian mass extinction. Nature Comm. 8, 164. https://doi.org/10.1038/s41467-017-00083-9.

Campbell, I.H., Griffiths, R.W., Hill, R.I., 1989. Melting in an Archaean mantle plume: heads it's basalts, tails it's komatiites. Nature 339 (6227), 697–699.

Campbell, I.H., Griffiths, R.W., 1990. Implications of mantle plume structure for the evolution of flood basalts. Earth Planet. Sci. Lett. 99 (1-2), 79–93.

Chowdhury, P., Chakraborty, S., Gerya, T.V., Cawood, P.A., Capitanio, F.A., 2020. Peel-back controlled lithospheric convergence explains the secular transitions in Archean metamorphism and magmatism. Earth Planet. Sci. Lett. 538, 116224. https://doi.org/10.1016/j.epsl.2020.116224.

Christensen, U.R., 1985. Thermal evolution models for the Earth. J. Geophys. Res. 90 (B4), 2995. https://doi.org/10.1029/JB090iB04p02995.

Ciborowski, T.J.R., Minifie, M.J., Kerr, A.C., Ernst, R.E., Baragar, B., Millar, I.L., 2017. A mantle plume origin for the Palaeoproterozoic circum-superior large Igneous Province. Precambrian Res. 294, 189–213.

Coffin, M.F., Eldholm, O., 1994. Large igneous provinces: crustal structure, dimensions, and external consequences. Rev Geophys. 32 (1), 1. https://doi.org/10.1029/93RG02508.

Condie, K.C., Pisarevsky, S.A., Puetz, S.J., 2021. LIPs, orogens and supercontinents: The ongoing saga. Gondwana Res. 96, 105–121.

Connolly, B.D., Puchtel, I.S., Walker, R.J., Arevalo, R., Piccoli, P.M., Byerly, G., Robin-Popieul, C., Arndt, N., 2011. Highly Siderophile Element systematics of the 3.3 Ga Weltevreden komatiites, South Africa: implications for early Earth history. Earth Planet. Sci. Lett. 311 (3-4), 253–263.

Coogan, L.A., Saunders, A.D., Wilson, R.N., 2014. Aluminum-in-olivine thermometry of primitive basalts: evidence of an anomalously hot mantle source for large igneous provinces. Chem. Geol. 368, 1–10. https://doi.org/10.1016/j.chemgeo.2014.01.004.

Corrigan, D., Pehrsson, S., Wodicka, N., de Kemp, E., 2009. The Palaeoproterozoic Trans-Hudson Orogen: a prototype of modern accretionary processes. Geological Society, London, Special Publications 327 (1), 457–479.

Courtillot, V., Jaupart, C., Manighetti, I., Tapponnier, P., Besse, J., 1999. On causal links between flood basalts and continental breakup. Earth Planet. Sci. Lett. 166 (3-4), 177–195.

Coueslan, C.G., David R.M. Pattison, D.R.M, Dufrane, S.A., 2013. Paleoproterozoic metamorphic and deformation history of the Thompson Nickel Belt, Superior Boundary Zone, Canada, from in situ U–Pb analysis of monazite. Precamb. Res. 237, 13-35.

Dalton, C.A., Langmuir, C.H., Gale, A., 2014. Geophysical and Geochemical Evidence for Deep Temperature Variations Beneath Mid-Ocean Ridges. Science 344 (6179), 80–83.

Davies, G.F., 1980. Thermal histories of convective Earth models and constraints on radiogenic heat production in the Earth. J. Geophys. Res. 85 (B5), 2517. https://doi.org/10.1029/JB085iB05p02517.

Davies, J.H.F.L., Marzoli, A., Bertrand, H., You, N. Ernesto, M., Greber, N.D. Ackerson, M., Simpson, G., Bouvier, A.-S., Baumgartner, L., Pettke, T., Farina, F., Ahrenstedt, H.V., Schaltegger, U. 2021. Zircon petrochronology in large igneous provinces reveals upper crustal contamination processes: new U–Pb ages, Hf and O isotopes, and trace elements from the Central Atlantic magmatic province (CAMP). Contrib. Mineral. Petrol. 176:9. https://doi.org/10.1007/s00410-020-01765-2.

Davies, G.F., 2009. Effect of plate bending on the Urey ratio and the thermal evolution of the mantle. Earth Planet. Sci. Lett. 287, 513–518.

Davis, F.A., Hirschmann, M.M., Humayun, M., 2011. The composition of the incipient partial melt of garnet peridotite at 3GPa and the origin of OIB. Earth Planet. Sci. Lett. 308 (3-4), 380–390.

Desharnais, G., Peck, D.C., Halden, N.M., Scoates, R.F.J., Hulbert, L.J., 2004. Geochemical constraints on the tectonomagmatic evolution of the Fox River Belt, northeastern Manitoba (NTS 53M15 and 16); Manitoba Industry. Economic Development and Mines, Manitoba Geological Survey, Geoscientific Paper GP2004-1 33, p.

Ernst, R.E., Buchan, K.L., 2004. Igneous rock association in Canada 3. Large Igneous Provinces (LIPs) in Canada and adjacent regions: 3 Ga to present. Geosci. Can. 31, 103–126.

Ernst, R., Bleeker, W., 2010. Large igneous provinces (LIPs), giant dyke swarms, and mantle plumes: significance for breakup events within Canada and adjacent regions from 2.5 Ga to the present. Canadian. J. Earth Sci. 47 (5), 695–739.

Falloon, T.J., Danyushevsky, L.V., 2000. Melting of refractory mantle at 1.5, 2 and 2.5 GPa under anhydrous and $H_2O$-undersaturated conditions: implications for the petrogenesis of high-Ca boninites and the influence of subduction components on mantle melting. J. Petrol. 41, 257–283.

Fan, J., Kerrich, R., 1997. Geochemical characteristics of aluminum depleted and undepleted komatiites and HREE-enriched low-Ti tholeiites, Western Abitibi greenstone belt: a heterogeneous mantle plume-convergent margin environment. Geochim. Cosmochim. Acta 61 (22), 4723–4744.

Farnetani, C.G., Samuel, H., 2005. Beyond the thermal plume paradigm. Geophys. Res. Lett. 32 (7) https://doi.org/10.1029/2005GL022360.

Francis, D., Ludden, J., Hynes, A., 1983. Magma evolution in a proterozoic rifting environment. J. Petrol. 24 (4), 556–582.

French, J.E., Heaman, L.M., Chacko, T., Srivastava, R.K., 2008. 1891–1883 Ma Southern Bastar-Cuddapah mafic igneous events, India: a newly recognized large igneous province. Precambr. Res. 160, 308–322.

Gaborieau, M., Laubier, M., Bolfan-Casanova, N., McCammon, C.A., Vantelon, D., Chumakov, A.I., Schiavi, F., Neuville, D.R., Venugopal, S., 2020. Determination of $Fe^{3+}/\Sigma Fe$ of olivine-hosted melt inclusions using Mössbauer and XANES spectroscopy. Chem. Geol. 547, 119646. https://doi.org/10.1016/j.chemgeo.2020.119646.

Ganne, J., Feng, X., 2017. Primary magmas and mantle temperatures through time. Geochem. Geophys. Geosyst. 18 (3), 872–888.

Ghiorso, M.S., Sack, R.O., 1995. Chemical mass transfer in magmatic processes IV. A revised and internally consistent thermodynamic model for the interpolation and extrapolation of liquid-solid equilibria in magmatic systems at elevated temperatures and pressures. Contrib. Mineral. Petrol. 119 (2-3), 197–212.

Göğüş, O.H., Ueda, K., 2018. Peeling back the lithosphere: Controlling parameters, surface expressions and the future directions in delamination modeling. J. Geodynamics 117, 21–40.

Gomes, A.S., Vasconcelos, P.M., 2021. Geochronology of the Paraná-Etendeka large igneous province. Earth-Sci. Rev. 220, 103716. https://doi.org/10.1016/j.earscirev.2021.103716.

Gualda, G.A.R., Ghiorso, M.S., Lemons, R.V., Carley, T.L., 2012. Rhyolite-MELTS: a Modified Calibration of MELTS Optimized for Silica-rich, Fluid-bearing Magmatic Systems. J. Petrol. 53 (5), 875–890.

Hamilton, M.A., Stott, G.M., 2008. Project Unit 04-018. The significance of new U/Pb baddeleyite ages from two Paleoproterozoic diabase dikes in northern Ontario. In: Summary of Fieldwork and Other Activities 2008. Ontario Geological Survey Open File Report 6226. Ministry of Northern Development and Mines, Toronto. 17-1–17-7.

Hanski, E., Huhma, H., Rastas, P., Kamenetsky, 2001. The Palaeoproterozoic komatiite–picrite association of Finnish Lapland. J. Petrol. 42, 855–876.

Heaman, L.M., Machado, N., Krogh, T.E., Weber, W., 1986. Precise U-Pb zircon ages for the Molson dyke swarm and the Fox River sill: constraints for early Proterozoic crustal evolution in northeastern Manitoba. Canada. Contrib. Miner. Petrol. 94 (1), 82–89.

Heaman, L.M., Peck, D., Toope, K., 2009. Timing and geochemistry of 1.88 Ga Molson Igneous Events, Manitoba: insights into the formation of a craton-scale magmatic and metallogenic province. Precambr. Res. 172 (1-2), 143–162.

Herzberg, C., 1992. Depth and degree of melting of komatiites. J. Geophys. Res. 97 (B4), 4521. https://doi.org/10.1029/91JB03066.

Herzberg, C., 1995. Generation of plume magmas through time: an experimental perspective. Chem. Geol. 126 (1), 1–16.

Herzberg, C., 2006. Petrology and thermal structure of the Hawaiian plume from Mauna Kea volcano. Nature 444, 605–609.

Herzberg, C., 2011. Identification of Source Lithology in the Hawaiian and Canary Islands: Implications for Origins. J. Petrol. 52, 113–146.

Herzberg, C., 2019. Origin of high-Mg bimineralic eclogite xenoliths in kimberlite: A comment on a paper by Aulbach and Arndt (2019). Earth Planet. Sci. Lett. 510, 231–233.

Herzberg, C., O'Hara, M.J., 2002. Plume-associated ultramafic magmas of phanerozoic age. J. Petrol. 43, 1857–1883.

Herzberg, C., Gazel, E., 2009. Petrological evidence for secular cooling in mantle plumes. Nature 458, 619–622.

Herzberg, C., Asimow, P.D., 2008. Petrology of some oceanic island basalts: PRIMELT2.XLS software for primary magma calculation. Geochem. Geophys. Geosyst. 8, Q09001. https://doi.org/10.1029/2008GC002057.

Herzberg, C., Asimow, P.D., 2015. PRIMELT3 MEGA.XLSM software for Primary Magma Calculation: Peridotite Primary Magma MgO Contents from the Liquidus to the Solidus. Geochem. Geophys. Geosys. 16, 563–578. https://doi.org/10.1002/2014G005631.

Herzberg, C., Condie, K., Korenaga, J., 2010. Thermal evolution of the Earth and its petrological expression. Earth Planet. Sci. Lett. 292, 79–88.

Herzberg C., Asimow, P.D., Arndt, N. Niu, Y. Lesher, C.M., Fitton, J.G., Cheadle, M.J., Saunders, A.D. 2007. Temperatures in ambient mantle and plumes: Constraints from basalts, picrites and komatiites. Geochem. Geophys. Geosyst. 8, Q02006. 10.1029/2006GC001390.

Hulbert, L.J., Hamilton, M.A., Horan, M.F., Scoates, R.F.J., 2005. U-Pb zircon and Re-Os isotope geochronology of mineralized ultramafic intrusions and associated nickel ores of the Thompson Nickel Belt, Manitoba. Canada. Econ. Geol. 100, 29–41.

Hynes, A., Francis, D.M., 1982. A transect of the early Proterozoic Cape Smith foldbelt, New Quebec. Tectonophysics 88, 23–59.

Jarvis, G.T., Campbell, I.H., 1983. Archean komatiites and geotherms: solution to an apparent contradiction. Geophys. Res. Lett. 10, 1133–1136.

Jennings, E.S., Holland, T.J.B., 2015. A Simple Thermodynamic Model for Melting of Peridotite in the System NCFMASOCr. J. Petrol. 56, 869–892.

Jennings, E.S., Gibson, S.A., Maclennan, J., 2019. Hot primary melts and mantle source for the Parana-Etendeka flood basalt province: New constraints from Al-in-olivine thermometry. Chem. Geol. 529, 119287. https://doi.org/10.1016/j.chemgeo.2019.119287.

Johnson, T.E., Brown, M., Kaus, B., Van Tongeren, J.A., 2014. Delamination andrecycling of Archaean crust caused by gravitational instabilities. Nat. Geosci. 7, 47–52.

Kasbohm, J., Schoene, B., 2018. Rapid eruption of the Columbia River flood basalt and correlation with the mid-Miocene climate optimum. Sci. Adv. 4, eaat8223.
Kamo, S.L., Czamanske, G.K., Amelin, Y., Fedorenko, V.A., Davis, D.W., Trofimov, V.R., 2003. Rapid eruption of Siberian food-volcanic rocks and evidence for coincidence with the Permian-Triassic boundary and mass extinction at 251 Ma. Earth Planet. Sci. Lett. 214, 75–91.
Kastek, N., Ernst, R.E., Cousens, B.L., Kamo, S.L., Bleeker, W., Söderlund, U., Baragar, W. R.A., Sylvester, P., 2018. U-Pb geochronology and geochemistry of the Povungnituk Group of the Cape Smith Belt: part of a Craton-Scale Circa 2.0 Ga Minto-Povuntnituk large Igneous Province. Northern Superior Craton. Lithos 320–321, 315–331.
Kastek, N., Mungall, J.E., Ernst, R.E., Cousens, B.L., 2020. Roberts Lake Syncline mafic lavas (NE Superior craton): A proposed extension of the Cape Smith belt. Lithos 366–367. https://doi.org/10.1016/j.lithos.2020.105545.
Kerr, A.C., Saunders, A.D., Tarney, J., Berry, N.H., Hards, V.L., 1995. Depleted mantle-plume geochemical signatures: No paradox for plume theories. Geology 23, 843–846.
Kress, V.C., Carmichael, I.S.E., 1991. The compressibility of silicate liquids containing $Fe_2O_3$ and the effect of composition, temperature, oxygen fugacity and pressure on their redox States. Contrib. Mineral. Petrol. 108, 82–92.
Korenaga, J., 2008. Urey ratio and the structure and evolution of Earth's mantle. Rev. Geophys. 46, RG2007. https://doi.org/10.1029/2007RG000241.
Lahaye, Y., Arndt, N.T., 1996. Alteration of a komatiitic flow: Alexo, Ontario, Canada. J. Petrol. 37, 1261–1284.
Langmuir, C.H., Klein, E.M., Plank, T., 1992. Petrological systematics of Mid-Ocean Ridge Basalts: constraints on melt generation beneath ocean ridges. In Mantle Flow and Melt Generation at Mid-Ocean Ridges, Geophys. Monogr. Ser. 71, edited by Morgan, J.P, Blackman, D.K. and J.M. Sinton, J.M. 183-280, AGU, Washington DC.
Larsen, L.M., Pedersen, A.K., Tegner, C., Duncan, R.A., Hald, N., Larsen, J., 2016. Age of Tertiary volcanic rocks on the West Greenland continental margin: volcanic evolution and event correlation to other parts of the North Atlantic Igneous Province. Geol. Mag. 153, 487–511. https://doi.org/10.1017/S0016756815000515.
Larsen, L.M., Williamson, M.-C., 2020. Depleted and ultradepleted basalt and picrite in the Davis Strait: Paleocene volcanism associated with a transform continental margin. Geol. Mag. 157, 1983–2003. https://doi.org/10.1017/S0016756820000175.
Matthews, S., Wong, K., Shorttle, O., Edmonds, M., Maclennan, J. 2021. Do Olivine Crystallization Temperatures Faithfully Record Mantle Temperature Variability? Geochem. Geophys. Geosys. 22, e2020GC009157. https://doi.org/10.1029/2020GC009157.
Matzen, A.K., Baker, M.B., Beckett, J.R., Stolper, E.M., 2011. Fe-Mg partitioning between olivine and high-magnesian melts and the nature of Hawaiian parental liquids. J. Petrol. 52, 1243–1263.
Matzen, A.K., Baker, M.B., Beckett, J.R., Stolper, E.M., 2013. The temperature and pressure dependence of nickel partitioning between olivine and silicate melt. J. Petrol. 54, 2521–2545.
Matzen, A.K., Baker, M.B., Beckett, J.R., Wood, B.J., Stolper, E.M., 2017. The effect of liquid composition on the partitioning of Ni between olivine and silicate melt. Contrib. Mineral. Petrol. 172, 3. https://doi.org/10.1007/s00410-016-1319-8.
McKenzie, D., 1984. The generation and compaction of partial melts. J. Petrol. 25, 713–765.
McKenzie, D., Bickle, M.J., 1988. The volume and composition of melt generated by extension of the lithosphere. J. Petrol. 29, 625–679.
Medard, E., Grove, T.L., 2008. The effect of H2O on the olivine liquidus of basaltic melts: experiments and thermodynamic models. Contrib. Mineral. Petrol. 155, 417–432.
Minifie, M.J., Kerr, C.K., Ernst, R.E., Hastie, A.R., Ciborowski, T.J.R., Desharnais, G., Millar, I.L., 2013. The northern and southern sections of the western ca. 1880 Ma Circum- Superior large Igneous Province, North America: the Pickle Crow dyke connection? Lithos 174, 217–235.
Moussallam, Y., Longpré, M.-A., McCammon, C., Gomez-Ulla, A., Rose-Koga, E.F., Scaillet, B., Peters, N., Gennaro, E., Paris, R., Oppenheimer, C., 2019. Mantle plumes are oxidized. Earth Planet. Sci. Lett. 527, 115798.
Nicklas, R.W., Puchtel, I.S., Ash, R.D., Piccoli, P., Hanski, E., Nisbet, E.G., Waterton, P., Pearson, D.G., Anbar, A.D., 2019. Secular mantle oxidation across the Archean-Proterozoic boundary: evidence from V partitioning in komatiites and picrites. Geochim. Cosmochim. Acta 250, 49–75.
Nisbet, E.G., Cheadle, M.J., Arndt, N.T., Bickle, M.J., 1993. Constraining the potential temperature of the Archaean mantle: review of the evidence from komatiites. Lithos 30, 291–307.
Parman, S.W., Grove, T.L., Dann, J.C., de Wit, M.J., 2004. A subduction origin for komatiites and cratonic lithospheric mantle. S. Afr. J. Geol. 107 (1–2), 107–118.
Petterson, M.G., Babbs, T., Neal, C.R., Mahoney, J.J., Saunders, A.D., Duncan, R.A., Tolia, D., Magua, R., Qopoto, C., Mahoaa, H., Natogga, D., 1999. Geological–tectonic framework of Solomon Islands, SW Pacific: crustal accretion and growth within an intra-oceanic setting. Tectonophysics 301, 35–60.
Percival, J.A., Whalen, J.B., Rayner, N., 2005. Pikwitonei–Snow Lake Manitoba transect (parts of NTS 63J, 63O and 63P), Trans-Hudson Orogen–Superior Margin Metallotect Project: new results and tectonic interpretation. In Report of Activities 2005, Manitoba Industry, Economic Development and Mines, Manitoba Geological Survey, pp. 69–91.
Picard, C., 1989. Lithochimie des roches volcaniques ProtCrozoiques de la partie occidentale de la fosse de l'Ungava (region au sud du lac Lanyan). Ministre de 1′ Energie et des Ressources du Quebec, ET 87-14.
Robin-Popieul, C.C.M., Arndt, N.T., Chauvel, C., Byerly, G.R., Sobolev, A.V., Wilson, A., 2012. A new model for Barberton komatiites: deep critical melting with high melt retention. J. Petrol. 53, 2191–2229.
Puchtel, I.S., Humayun, M., Campbell, A.J., Sproule, R.A., Lesher, C.M., 2004. Platinum group element geochemistry of komatiites from the Alexo and Pyke Hill areas, Ontario, Canada. Geochim. Cosmochim. Acta 68, 1361–1383.
Puchtel, I.S., Walker, R.J., Brandon, A.D., Nisbet, E.G., 2009. Pt-Re-Os and Sm-Nd isotope and HSE and REE systematic of the 2.7 Ga Belingwe and Abitibi komatiites. Geochem. Cosmochim. Acta 73, 6367–6389.
Puchtel, I.S., Blichert-Toft, J., Touboul, M., Walker, R.J., Byerly, G.R., Nisbet, E.G., Anhaeusser, C.R., 2013. Insights into early Earth from Barberton komatiites: Evidence from lithophile isotope and trace element systematics. Geochim. Cosmochim. Acta 108, 63–90.
Puchtel, I.S., Mundl-Petermeier, A., Horan, M., Hanski, E.J., Blichert-Toft, J., Walker, R. J., 2020. Ultra-depleted 2.05 Ga komatiites of Finnish Lapland: Products of grainy late accretion or core-mantle interaction? Chem. Geol. 554, 119801. https://doi.org/10.1016/j.chemgeo.2020.119801.
Puchtel, I.S., Blichert-Toft, J., Horan, M.F., Touboul, M., Walker, R.J., 2022. The komatiite testimony to ancient mantle heterogeneity. Chem. Geol. 594 https://doi.org/10.1016/j.chemgeo.2022.120776.
Putirka, K.D., Perfit, M., Ryerson, F.J., Jackson, M.G., 2007. Ambient and excess mantle temperatures, olivine thermometry, and active vs. passive upwelling. Chem. Geol. 241, 177–206.
Randall, W., 2005. U-Pb Geochronology of the Expo Intrusive Suite, Cape Smith Belt, and the Kyak Bay Intrusion, New Quebec Orogen: Implications for the Tectonic Evolution of the Northeastern Trans-Hudson Orogen. University of Toronto. M.Sc. thesis.
Richards, M.A., Duncan, R.A., Courtillot, V.E., 1989. Flood basalts and hotspot tracks: Plumes heads and tails. Science 246, 103–107.
Richter, F.M., 1985. Models for the Archean thermal regime. Earth Planet. Sci. Lett. 73, 350–360.
Roeder, P.L., Emslie, R.F., 1970. Olivine-liquid equilibrium. Contrib. Miner. Petrol. 29, 275–289.
Saunders, A.D., Fitton, J.G., Kerr, A.C., Norry, M.J., Kent, R.W., 1997. The North Atlantic Igneous Province. In Mahoney, J.J., Coffin, M.F. (Eds.), Large Igneous Provinces: Continental, Oceanic, and Planetary Flood Volcanism. Geophysical Monograph 100. AGU, Washington DC, 45–93.
Scoates, R.F.J., 1990, The Fox River Sill, northeastern Manitoba; a major stratiform intrusion; Manitoba Energy and Mines, Geological Report GR82-3, 192 p.
Scoates, R.F.J., Macek, J.J., 1978. MolsonDyke Swarm.Manitoba Department of Energy and Mines Geological Paper 78-1, 53 pp.
Scoates, J.S., Scoates, R.J., Wall, C.J., Friedman, R.M., Coueslan, C.G., 2017. Direct dating of ultramafic sills and mafic intrusions associated with Ni-sulphide mineralization in the Thompson Nickel Belt, Manitoba, Canada. Econ. Geol. 112, 675–692.
Schoene, B., Eddy, M.P., Samperton, K.M., Keller, B., Keller, G., Adatte, T., Khadri, S.F.R., 2019. U-Pb constraints on pulsed eruption of the Deccan Traps across the end-Cretaceous mass extinction. Science 363, 862–866.
Shore, M., 1996. Cooling and crystallization of komatiite flows. University of Ottawa. Ph. D. thesis.
Sleep, N.H., 2008. Channeling at the base of the lithosphere during the lateral flow of plume material beneath flow line hot spots. Geochem. Geophys. Geosys. 9, Q08005. https://doi.org/10.1029/2008GC002090.
Sleep, N.H., Ebinger, C.J., Kendall, J.-M., 2002. Deflection of mantle plume material by cratonic keels. In: The early Earth: physical, chemical and biological development. In: Fowler, C.M.R., Ebinger, C.J., Hawkesworth, C.J. (Eds.), Geological Society Special Publication, vol. 199. Geological Society of London, London, pp. 135–150.
Sobolev, A.V., Asafov, E.V., Gurenko, A.A., Arndt, N.T., Batanova, V.G., Portnyagin, M. V., Garbe-Schönberg, D., Krasheninnikov, S.P., 2016. Komatiites reveal a hydrous Archaean deep-mantle reservoir. Nature 531, 628–632.
Spencer, C.J., Mitchell, R.N. Brown, M., 2021. Enigmatic Mid-Proterozoic Orogens: Hot, Thin, and Low. Geophys. Res. Lett. 48. e2021GL093312. https://doi.org/10.1029/2021GL093312.
Sobolev, A.V., Asafov, E.V., Gurenko, A.A., Arndt, N.T., Batanova, V.G., Portnyagin, M. V., Garbe-Schönberg, D., Wilson, A.H., Byerly, G.B., 2019. Deep hydrous mantle reservoir provides evidence for crustal recycling before 3.3 billion years ago. Nature 571, 555–559. https://doi.org/10.1038/s41586-019-1399-5.
Spice, H.E., Fitton, J.G., Kirstein, L.A., 2016. Temperature fluctuation of the Iceland mantle plume through time. Geochem. Geophys. Geosys. 17 (2), 243–254. https://doi.org/10.1002/2015GC006059.
Sprain, C.J., Renne, P.R., Vanderkluysen, L., Pande, K., Self, S., Mittal, T., 2019. The eruptive tempo of Deccan volcanism in relation to the Cretaceous-Paleogene boundary. Science 363, 866–870.
Sproule, R.A., Lesher, C.M., Ayer, J.A., Thurston, P.C., Herzberg, C.T., 2002. Spatial and temporal variations in the geochemistry of komatiites and komaiitic basalts in the Abitibi greenstone belt. Precamb. Res. 115, 153–186.
Storey, B.C., 1995. The role of mantle plumes in continental breakup: case histories from Gondwanaland. Nature 377, 301–308.
Sugawara, T., 2000. Empirical relationships between temperature, pressure, and MgO content in olivine and pyroxene saturated liquid. J. Geophys. Res. 105, 8457–8472.
Svensen, H., Fernando Corfu, F., Polteau, S., Hammer, Ø., Planke, S., 2012. Rapid magma emplacement in the Karoo Large Igneous Province. Earth Planet. Sci. Lett. 325–326, 1–9.
Tomlinson, E., Holland, T.J.B., 2021. A thermodynamic model for the subsolidus evolution and melting of peridotite. J. Petrol. 62, 1–23.
Toplis, M.J., 2005. The thermodynamics of iron and magnesium partitioning between olivine and liquid: criteria for assessing and predicting equilibrium in natural and experimental systems. Contrib. Mineral. Petrol. 149, 22–39.

Trela, J., Gazel, E., Sobolev, A.V., Moore, L., Bizimis, M., Jicha, B., Batanova, V.G., 2017. The hottest lavas of the Phanerozoic and the survival of deep Archaean reservoirs. Nat. Geosci. 10 (6), 451.

Trela, J., Vidito, C., Gazel, E., Herzberg, C., Class, C., Whalen, W., Jicha, B., Bizimis, M., Avarado, G.E., 2015. Recycled crust in the Galapagos plume source at 70 Ma: Implications for plume evolution. Earth Planet. Sci. Lett. 425, 268–277.

Ueki, K., Kuwatania, T., Okamotoc, A., Akahod, S., Iwamoria, H., 2020. Thermodynamic modeling of hydrous-melt–olivine equilibrium using exhaustive variable selection. Phys. Earth Planet. Inter. 300 https://doi.org/10.1016/j.pepi.2020.106430.

Walter, M.J., 1998. Melting of garnet peridotite and the origin of komatiite and depleted lithosphere. J. Petrol. 39, 29–60.

Wan, B., Yang, X., Tian, X., Yuan, H., Kirscher, U., Mitchell, R.N., 2020. Seismological evidence for the earliest global subduction network at 2 Ga ago. Sci. Adv. 6, eabc5491.

Waterton, P., Person, D.G., Kjarsgaard, B., Hulbert, L., Locock, A., Parman, S., David, D., 2017. Age, origin, and thermal evolution of the ultra-fresh ~1.9 Ga Winnipegosis Komatiites, Manitoba, Canada. Lithos 268–271, 114–130.

Wilson, A., 2019. The Late-Paleoarchean Ultra-Depleted Commondale Komatiites: Earth's Hottest Lavas and Consequences for Eruption. J. Petrol. 60, 1575–1620.

Wilson, A., Bolhar, R., 2021, Olivine in komatiite records origin and travel from the deep upper mantle. Geology 50, 351–355. https://doi.org/10.1130/G49523.1.

Xu, Y., Yang, Z., Tong, Y.-B., Jing, X., 2018. Paleomagnetic Secular Variation Constraints on the Rapid Eruption of the Emeishan Continental Flood Basalts in Southwestern China and Northern Vietnam. J. Geophys. Res. Solid Earth 123, 2597–2617. https://doi.org/10.1002/2017JB014757.

Zhao, G., Cawood, P.A., Wilde, S.A., Sun, M., 2002. Review of global 2.1–1.8 Ga orogens: implications for a pre-Rodinia supercontinent. Earth-Sci. Rev. 59, 125–162.

Zwanzig, H.V., 2005. Geochemistry, Sm–Nd isotope data and age constraints of the Bah Lake assemblage, Thompson Nickel Belt and Kisseynew Domain margin: relation to Thompson-type ultramafic bodies and a tectonic model (NTS 63J, O and P). Manitoba Geological Survey, Report of Activities 2005, 40–53.